Stem Cell Reports
Article

ISSCR

OPEN ACCESS

Human Neural Stem Cells Reinforce Hippocampal Synaptic Network and Rescue Cognitive Deficits in a Mouse Model of Alzheimer's Disease

Ting Zhang,[1,7] Wei Ke,[2,7] Xuan Zhou,[3,7] Yun Qian,[1] Su Feng,[1] Ran Wang,[1] Guizhong Cui,[1] Ran Tao,[1] Wenke Guo,[1,5] Yanhong Duan,[3] Xiaobing Zhang,[4] Xiaohua Cao,[3] Yousheng Shu,[2] Chunmei Yue,[1,8,*] and Naihe Jing[1,5,6,8,*]

[1]State Key Laboratory of Cell Biology, CAS Center for Excellence in Molecular Cell Science, Shanghai Institute of Biochemistry and Cell Biology, Chinese Academy of Sciences, University of Chinese Academy of Sciences, 320 Yue Yang Road, Shanghai 200031, China
[2]State Key Laboratory of Cognitive Neuroscience and Learning & IDG/McGovern Institute for Brain Research, Beijing Normal University, 19 Xinjiekou Wai Street, Beijing 100875, China
[3]Key Laboratory of Brain Functional Genomics, Ministry of Education, Shanghai Key Laboratory of Brain Functional Genomics, School of Life Sciences, East China Normal University, Shanghai, China
[4]Division of Regenerative Medicine, Department of Medicine, Loma Linda University, Loma Linda, CA, 92350, USA
[5]School of Life Science and Technology, ShanghaiTech University, Shanghai 201210, China
[6]Institute for Stem Cell and Regeneration, Chinese Academy of Sciences, Beijing 100101, China
[7]Co-first author
[8]Co-senior author
*Correspondence: cmyue@sibcb.ac.cn (C.Y.), njing@sibcb.ac.cn (N.J.)
https://doi.org/10.1016/j.stemcr.2019.10.012

SUMMARY

Alzheimer's disease (AD) is characterized by memory impairments in its earliest clinical phase. The synaptic loss and dysfunction leading to failures of synaptic networks in AD brain directly cause cognitive deficits of patient. However, it remains unclear whether the synaptic networks in AD brain could be repaired. In this study, we generated functional human induced neural progenitor/stem cells (iNPCs) that had been transplanted into the hippocampus of immunodeficient wild-type and AD mice. The grafted human iNPCs efficiently differentiated into neurons that displayed long-term survival, progressively acquired mature membrane properties, formed graft-host synaptic connections with mouse neurons and functionally integrated into local synaptic circuits, which eventually reinforced and repaired the neural networks of host hippocampus. Consequently, AD mice with human iNPCs exhibited enhanced synaptic plasticity and improved cognitive abilities. Together, our results suggest that restoring synaptic failures by stem cells might provide new directions for the development of novel treatments for human AD.

INTRODUCTION

Alzheimer's disease (AD) is the most prevalent form of dementia and currently remains incurable (Hurd et al., 2013). AD is pathologically characterized by progressively emerged amyloid-β (Aβ) aggregation, tau-rich neurofibrillary tangles and extensive synaptic disruption and neuronal loss in the patient brain. The leading theory in the field postulated that Aβ accumulation in brain regions important for memory and cognition initiates AD (Hardy and Selkoe, 2002), which provides clues for drug discovery for the treatment of AD. Over three decades, pharmaceutical companies have focused on Aβ plaques or tau tangles and developed drugs to remove plaques or stop them from forming. However, several promising drugs targeting Aβ or tau failed to rescue the cognitive deficits of AD patients or delay the progression of the disease in recent clinical trials (Cacabelos, 2018; Doody et al., 2014).

The Aβ-induced synaptic dysfunction and loss occur at an early stage of AD and form a fundamental part of the pathological process of the disease (Palop and Mucke, 2010). Evidence implicates that the synaptic failures directly affected the synaptic and neural circuits, which in turn caused irreversible impairments of cognitive function emerging in the earliest clinic phase of AD patients (Davies et al., 1987; Palop and Mucke, 2010; Selkoe, 2002). Then, it is therapeutically attractive to repair the disrupted synapse and reinforce synaptic networks, which might reverse the cognitive deficits of AD and provide a meaningful clinical benefit. The global neural degeneration in the brain of AD makes people believe that it is challenging to treat AD using cell replacement strategies. Efforts to explore the possibilities of repairing synaptic damages in AD brain by cell replacement have been limited. Previous studies suggested that the transplantation of mesenchymal stem cells or fetal brain tissue-derived human neural stem cells rescued memory deficits by reducing neuronal apoptosis (Lee et al., 2010) or promoting expression of synaptic markers of AD animals (Ager et al., 2015). Several other studies reported the improvement of cognitive abilities of AD animals upon transplantation of human or mouse neural stem cells from embryonic stem cells (ESCs) or iPSCs but did not measure the neurochemical changes of synapses in host brains (Liu et al., 2013; Moghadam et al., 2009). Our previous study suggested that the grafted mouse ESC-derived basal forebrain cholinergic neurons (BFCNs) formed synapses with host neural cells, displayed electrophysiological activity in the host brains and

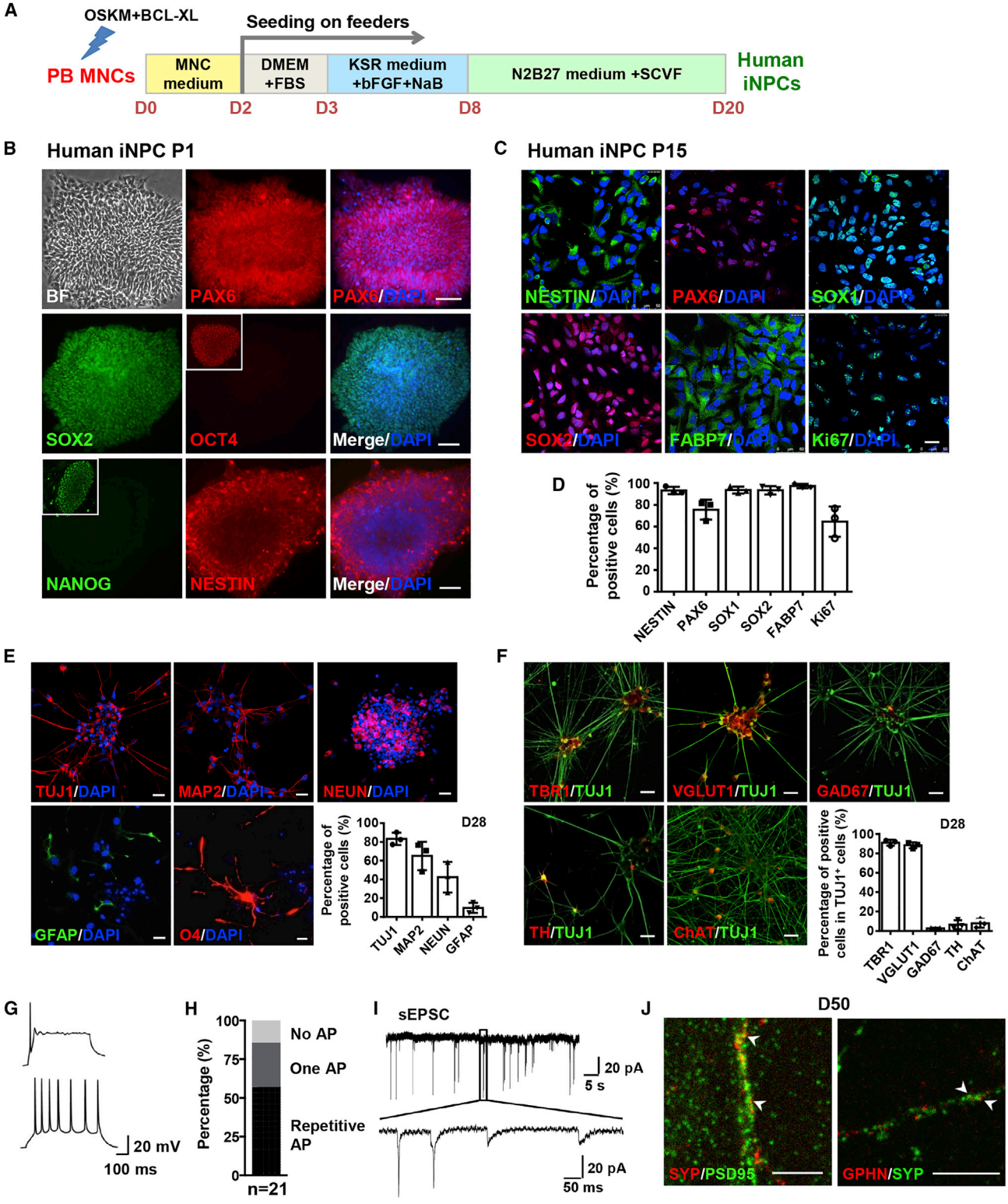

Figure 1. The Characterization of Human iNPCs Converted from a Small Volume of Peripheral Blood

(A) Schematic representation of the approach used to direct the conversion of PB MNCs into iNPCs.

(B) Immunofluorescence analysis of human iNPCs at passage 1. Note the representative OCT4^{+} and NANOG^{+} iPSC colonies in outlined regions as positive controls.

(legend continued on next page)

improved the cognitive ability of AD mice (Yue et al., 2015). These observations direct our attention to detect whether human neural progenitors or neurons could functionally integrate into local neural circuitry and reinforce synaptic connectivity in AD brain.

Human neural stem cells provide a potentially unlimited source of different neural cell types on demands to repair the degenerated or injured brain. However, human adult neural stem cells persist into special niches of brain and are inaccessible (Gage, 2000). Hence, the *in vitro* generation and possible therapeutic applications of human induced neural stem/progenitor cells (iNPCs) are of special interest. The reprogramming from human somatic cells into human iNPCs resembling brain neural stem cells has been achieved in recent years (Brand and Livesey, 2011). However, the potential therapeutic use of the resulting human iNPCs has remained to be explored.

In this study, functional human iNPCs were produced from immobilized human peripheral blood cells and displayed typical properties of brain NPCs. After transplantation into the hippocampus of immunodeficient wild-type (WT) and AD mice, the human iNPCs rapidly differentiated into neurons and astrocytes that survived well up to 12 months. The human iNPC-derived neurons gradually possessed the mature membrane properties, received synaptic inputs and formed synaptic connections with mouse hippocampal neurons. Moreover, the AD mice exhibited enhanced synaptic plasticity and improved cognitive abilities upon human iNPC transplantation.

RESULTS

Functional Human iNPCs Were Generated from a Small Volume of Peripheral Blood

The approach used to generate iNPCs from immobilized adult peripheral blood mononuclear cells (PB MNCs) in this study is based on overexpression of four iPS factors (OCT4, SOX2, c-MYC, and KLF4) in combination with small molecules as shown in Figure 1A. In brief, erythroblasts in PB MNCs from 3 to 8 mL peripheral blood were expanded, transfected by episomal vectors containing four iPS factors and an anti-apoptotic factor BCL-XL, and then sequentially cultured in three different types of media for 8 days to initiate reprogramming of PB MNCs. Subsequently, cells were treated with a cocktail of four chemicals (SB431542, CHIR99021, VPA and Forskolin, SCVF) in N2B27 medium for neural fate conversion (Figure 1A). Finally, NPC-like colonies with distinct morphology appeared within 3 weeks (Figure S1A). These colonies homogeneously expressed the NPC markers PAX6, SOX2, and NESTIN but not the pluripotency markers OCT4 and NANOG at passage 1, indicating that the PB MNCs rapidly acquired a neural progenitor identity and converted into iNPCs (Figure 1B). The chemicals played critical roles during neural fate conversion and the generated NPC-like colonies rapidly lost their self-renewal ability and went into spontaneous differentiation without chemicals (Figure S1A). In contrast, the chemical-induced iNPCs remained stable during prolonged culture and sustained the homogeneous expression of NESTIN, PAX6, SOX1, SOX2, FABP7, and the proliferation marker Ki67 at passage 15 (Figures 1C and 1D). PCR analysis at passage 5 confirmed that the exogenous genes in episomal vectors were not inserted into the genome of iNPCs and the iNPCs were integration free (Figure S1B). The established iNPC lines have been expanded and serially passaged as single cells for over 25 passages with a normal karyotype and maintained the capacity to form neurosphere, indicative of the self-renewal ability of iNPCs (Figures S1C–S1E).

To gain further insights into the transcriptional profile and cellular identity of human iNPCs, global gene expression of iNPCs was determined by bulk RNA sequencing of two different iNPC lines at passages 15 and 25, respectively. The top 1,000 upregulated and downregulated differentially expressed genes in human iNPCs revealed a clear difference between the transcriptomes of PB MNCs and iNPCs, while a high similarity was observed among all

(C) Immunofluorescence analysis of human iNPCs at passage 15.
(D) Quantification of the results shown in (C).
(E) Immunofluorescence analysis of human iNPC-derived neurons and astrocytes as at day 28, and oligodendrocytes at day 35, respectively, and corresponding differentiation efficiency.
(F) Immunofluorescence analysis of the subtypes of human iNPC-derived neurons and corresponding differentiation efficiency at day 28.
(G) Representative traces of single AP (top) and repetitive AP firing (bottom) of human iNPC-derived neurons at day 50 in response to step current injection.
(H) Percentages of human iNPC-derived cells with no AP, single AP or repetitive firing.
(I) Representative traces of spontaneous EPSCs received at a holding potential of −70 mV by human iNPC-derived neurons at day 50.
(J) Immunofluorescence analysis of SYNAPTOPHYSIN (SYP) co-labeling with PSD95 or GEPHYRIN (GPHN) in human iNPC-derived neurons at day 50. Arrowheads indicate the co-localization of pre- and postsynaptic dots.
Cell nuclei were counterstained with DAPI. Scale bars, 100 μm (B), 25 μm (C, E, F), 5 μm (J). n = 3 independent experiments. Data are represented as scatterplots with mean ± SD. Related to Figures S1 and S2.

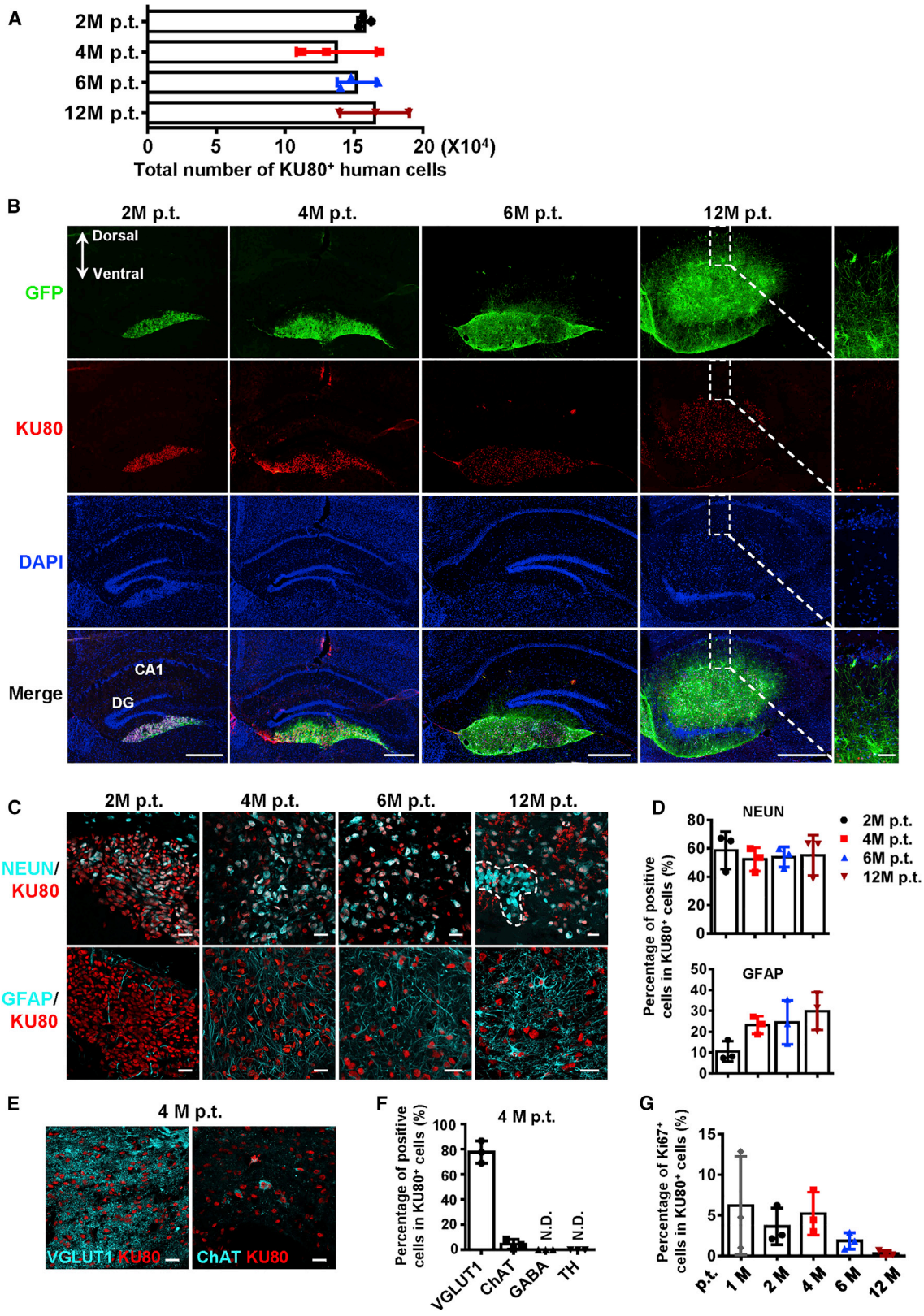

(legend on next page)

iNPC lines at different passages (Figures S2A–S2C). Gene ontology analysis showed that upregulated genes in iNPCs were mainly associated with neuronal differentiation and development (Figure S2C). These analyses confirmed that bona fide human iNPCs had been established and stably maintained *in vitro*. To further support this conclusion, we compared the global gene expression of human iNPCs with a published temporal transcriptome dataset of hESC-derived NPCs with prefrontal cortex identity (van de Leemput et al., 2014) and found that human iNPCs closely resembled hESC-derived NPCs at day 19 and 26 (Figure S2D). Hierarchical clustering analysis and scatterplots reflected that human iNPCs diverged from PB MNCs and closely clustered with hESC-derived NPCs (Figures S2E and S2F). In line with these findings, a comparative analysis with the database from BrainSpan Atlas of the Developing Human Brain showed that iNPCs mostly correlated with frontal cortex and ventral forebrain in fetal brain at 8 to 9 weeks (Figure S2G).

The potential of human iNPCs was assessed by their capacity to generate the three major neural lineages. Monolayer neural differentiation of human iNPCs gave rise robustly within 1 month of culture to neurons expressing neuronal marker genes TUJ1, MAP2, and NEUN as well as to astrocytes expressing GFAP, with larger numbers of neurons (Figure 1E). Differentiation toward oligodendrocytes was less efficient but some oligodendrocyte marker $O4^+$ cells with a typical oligodendrocytic morphology were observed (Figure 1E). Among the iNPC-derived $TUJ1^+$ neurons, over 90% were VGlut1-positive glutamatergic neurons expressing the cortical marker TBR1, but other subtypes of neurons, such as $GAD67^+$ GABAergic neurons, TH^+ dopaminergic neurons and $ChAT^+$ cholinergic neurons, were also found (Figure 1F). The whole-cell patch-clamp recordings revealed that iNPC-derived neurons possessed functional membrane properties by firing either one or repetitive action potentials (APs) (Figures 1G and 1H) and expressing excitatory postsynaptic currents (Figure 1I). The co-localization of presynaptic marker SYNAPTOPHYSIN with postsynaptic marker PSD95 revealed the existence of glutamatergic synapses or with GEPHYRIN for GABAergic synapses (Figure 1J).

Collectively, these results suggest a rapid conversion from PB MNCs to stable, homogeneous and self-renewing human iNPCs with a forebrain identity and the capacity to three major neural lineages.

The Human iNPCs Efficiently Differentiated into Neurons and Survived for Long-Term in the Brain of Host Mice

Next, we set out to investigate how human iNPCs function *in vivo* after transplantation. To this end, human iNPCs from donor $1^{\#}$ labeled with GFP at passage 15 were bilaterally transplanted into the hippocampus (10^5 cells per side, 2×10^5 cells per mouse) of immunodeficient $Foxn1^{-/-}$ mice (n = 39) by 2 months of age, which served as the WT control. The survival, migratory, differentiation and proliferation capacity of grafted iNPCs were determined 2, 4, 6, and 12 months after transplantation. The total number of grafted cells at each time point detected was around 1.5×10^5 (Figure 2A). GFP-positive grafted cells mainly located in hippocampus and extended long and abundant axons that projected into host dentate gyrus (DG) and CA1 region at 6 and 12 months (Figure 2B). All GFP^+ cells expressed KU80, a human-specific nuclear marker, and the $KU80^+$ human cells became more and more scattered from 2 to 12 months after transplantation (Figure S3A). One month after transplantation, majority of the $KU80^+$ iNPCs rapidly differentiated into $TUJ1^+$ neurons and $NESTIN^+$ NPCs were seldom detected (Figures S3B and S3C). Then, $KU80^+NEUN^+$ human neurons gradually migrated and mixed with the $KU80^-NEUN^+$ endogenous hippocampal granular cells (Figure 2C, top panel). The fraction of iNPC-derived mature neurons was relatively stable over time, accounting for approximately 60% of grafted $KU80^+$ cells (Figures 2C and 2D, top panels). In contrast, the differentiation of human iNPCs to astrocytes was slower. Double labeled $KU80^+GFAP^+$ astrocytes were detectable 2 months after transplantation and became a little abundant at 6 and 12 months (Figures 2C and 2D,

Figure 2. Differentiation of Grafted Human iNPCs in Hippocampus of Immunodeficient Mice

(A) Total numbers of $KU80^+$ human cells in the hippocampus of immunodeficient mice 2, 4, 6, and 12 months post transplantation (M p.t.).

(B) The coronal brain section harboring grafted GFP^+ human iNPCs at 2, 4, 6, and 12 M p.t. (Top) Immunofluorescence analysis of KU80 expression among GFP^+ cells (second panel). Cell nuclei were counterstained with DAPI.

(C) Immunofluorescence analysis of NEUN and GFAP expression in $KU80^+$ cells. The dashed line indicates the $KU80^-NEUN^+$ host neurons mixing with grafted cells.

(D) Percentages of $NEUN^+$ mature neurons and $GFAP^+$ astrocytes among $KU80^+$ grafted human cells shown in (C).

(E) Immunofluorescence analysis of subtypes of human iNPC-derived neurons among $KU80^+$ cells at 4 M p.t.

(F) Quantification of the results shown in (E).

(G) Percentages of $Ki67^+$ cells among $KU80^+$ grafted cells at 1, 2, 4, 6, and 12 M p.t. shown in Figure S3D.

Scale bars, 500 μm (B), 50 μm (magnified image in B) and 25 μm (C and E). n = 3 mice per time point. Data are represented as scatterplots with mean ± SD. Related to Figure S3.

bottom panels). Further analysis showed that the grafted human iNPCs predominantly gave rise to VGlut1$^+$ glutamatergic neurons as well as a few ChAT$^+$ cholinergic neurons and no other subtypes were detected (Figures 2E and 2F). Due to the quick differentiation of grafted iNPCs, the proliferation ability of human iNPCs dramatically decreased by lost expression of Ki67 and the graft overgrowth was not observed in the host brain. Only 5% of cells among grafted cells kept proliferating at 1 month after transplantation and the number decreased to 1% at 12 months (Figures 2G and S3D). These data suggest that human iNPCs rapidly stop proliferation and robustly differentiate into neurons and astrocytes in the host hippocampus. More importantly, the iNPC-derived human neurons have maintained viability for at least 12 months, gradually migrated and projected long and abundant axons into host hippocampus.

Human iNPC-Derived Neurons Gradually Matured in the Brain of Host Mice

We then examined whether transplanted human iNPC-derived neurons became functionally mature. To address this question, we performed whole-cell recording in brains obtained from host mice 2, 4, and 6 months after transplantation. GFP-positive grafted cells in acute slices were identified under a fluorescence microscope and recorded by patch pipettes with Alexa Fluor 594 (Figure 3A). Some of the recorded human iNPC-derived neurons generated spontaneous APs due to the depolarized resting membrane potential, displaying typical neuronal properties (Figure 3B). The resting membrane potential of the GFP$^+$ neurons gradually hyperpolarized and the input resistance progressively decreased in a time-dependent manner (Figure 3C). Larger current injections in neurons from 4- and 6-month, but not 2-month grafted brains induced repetitive firing without failure (Figure 3D), indicating that longer differentiating time promoted acquisition of mature membrane properties by human neurons in the host hippocampus. Consistently, 100% of the 4- and 6-month neurons recorded could generate APs and most of them discharged repetitively, while only ~50% of recorded 2-month neurons showed repetitive firing in response to step current injections (Figure 3E). The F-I curves of 4- and 6-month neurons exhibit gradual increases in AP frequency with increasing current injections from 20 to 180 pA and to 300 pA, respectively (Figure 3F). Currents greater than 180 pA for 4-month neurons and 300 pA for 6-month neurons caused inactivation of voltage-gated sodium channels and thus failure of repetitive firing. In sharp contrast, 2-month neurons could only generate repetitive APs within a small current range, from 20 to 60 pA (Figure 3F). Collectively, the electrophysiological profiles displayed by human iNPC-derived neurons showed that grafted human neurons gradually mature in the host hippocampus and acquire functional membrane properties around 6 months after transplantation.

Human iNPC-Derived Neurons Functionally Integrated into the Synaptic Network of the Host Hippocampus

The finding that human iNPC-derived neurons functionally matured *in vivo* prompted us to further examine whether they integrated into the synaptic circuitry of host hippocampus. In acute slices, all three groups of neurons (2, 4, and 6 months after transplantation) were recorded both spontaneous excitatory postsynaptic currents (sEPSCs) and inhibitory postsynaptic currents (sIPSCs) (Figure 4A), indicating that the grafted human neurons received synaptic inputs from other neurons, either other grafted cells or host cells. In addition, the decreases of rise time or decay time constant were in line with the maturation of neurons (Figures 4A and 4B) and the percentage of 6-month neurons exhibiting EPSCs was much higher than those of 2- or 4-month neurons (Figure 4C), indicative of increased synaptic transmission. To further investigate functional synaptic connections from grafted cells to host cells, we employed an optogenetic approach and transduced grafted human iNPCs with channelrhodopsin-2 (ChR2) tagged with mCherry (Figure 4D), so that grafted cells could be identified by their expression of mCherry. In voltage-clamp mode, we could obtain inward currents in these cells in response to blue light stimulation at the perisomatic region. As shown in Figure 4D, fast synaptic events occurred together with the relatively slow light-evoked current, indicating synaptic inputs from other grafted cells. These inward currents could induce trains of APs when cells were recorded in current-clamp mode (Figure 4D). Similar light stimulation could not evoke AP firing in neighboring host granular cells with unique firing pattern, but was able to cause an increase in the frequency of EPSCs of granule cells (7/21), showing that grafted cells synapse onto host cells (Figure 4E). Together, the detection of synapse transmission between grafted human neurons and host hippocampal neurons indicates the functional integration of grafted human neurons into the synaptic networks of the host hippocampus.

The Functional Integration of Human iNPC-Derived Neurons Reinforced the Synaptic Circuits of Hippocampus in the Brain of AD Mice

Given the functional integration of human iNPCs in WT immunodeficient mice, we next sought to determine whether they can also integrate in the brain of AD mice. To increase the survival of human iNPCs in the brain of AD mice, we crossed the well-established transgenic AD model 5XFAD mice with Rag2$^{-/-}$ mice, generating an

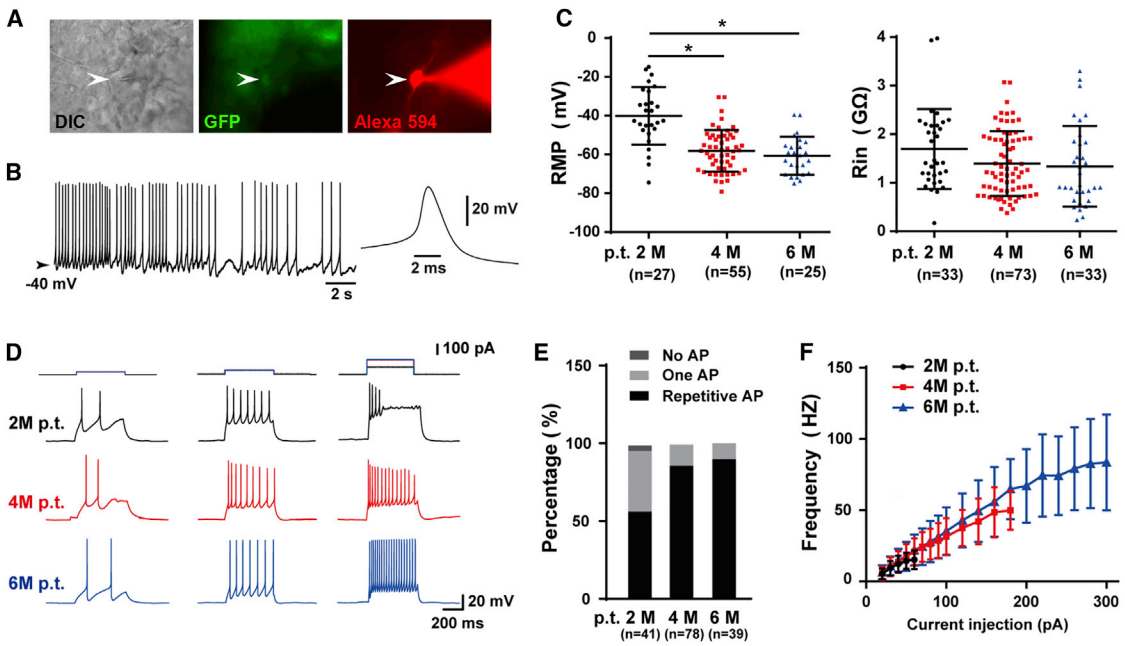

Figure 3. The Maturation of Grafted Human iNPC-Derived Neurons in Mice Hippocampus

(A) Representative human iNPC-derived neurons (arrowhead) in hippocampus on acute slice from brain of an immunodeficient mouse 2 M p.t. Left, DIC image; middle, GFP; right, filling the cell with Alexa Fluor 594 (100 μM) during whole-cell recording.

(B) Spontaneous APs recorded in some iNPC-derived neurons on acute slices. Inset, an expanded AP for clarity.

(C) The resting membrane potential of human neuronal cells gradually hyperpolarized after transplantation and the input resistance decreased in a time-dependent manner. Data are represented as scatterplots with mean ± SD. One-way ANOVA followed by Tukey's post-hoc test. *$p < 0.05$.

(D) AP generation in grafted human neuronal cells in responses to step current injection.

(E) Percentage of human neuronal cells with no AP, single AP, or repetitive AP at 2, 4, and 6 M p.t.

(F) Comparison of F-I curves from human neuronal cells at 2, 4, and 6 M p.t. Data are represented as scatterplots with mean ± SD. Sample size: 3 mice for 2 M p.t. and 6 M p.t. group, respectively; 6 mice for 4 M p.t. group. Numbers of recorded cells (n) were shown on the graphs in (C) and (E).

immunodeficient AD mouse line, $Rag2^{-/-}$/5XFAD. GFP-labeled iNPCs (passage 15) were bilaterally transplanted into hippocampus (10^5 cells per side) of 4-month-old $Rag2^{-/-}$/5XFAD mice with abundant Aβ plaques. Six months after transplantation, abundant GFP^+ grafted cells ($[13.2 \pm 2.8] \times 10^4$, n = 3) survived in the host hippocampus without any detectable graft overgrowth in the hippocampus or ectopic cell clusters in other regions of brain in $Rag2^{-/-}$/5XFAD mice examined (n = 22) (Figure 5A). Immunostaining analysis showed that the green grafted cells were surrounded by abundant Aβ plaques, but there were no detectable Aβ plaques among GFP^+ human cells (Figures 5A and 5B). The $KU80^+$ human iNPCs were found to differentiate into $NEUN^+$ mature neurons and in smaller numbers into $GFAP^+$ astrocytes (Figures 5B and S4A). The long green neurites from grafted human neurons projected into the host neural cells (Figure 5B). $Iba1^+$ microglia were exclusively associated with Aβ plaques but hardly detectable among GFP^+ human cells (Figure 5C). Whole-cell recording was performed in acute slices from AD brain 6 months after transplantation and spontaneous AP firing was detected in human iNPC-derived neurons (Figure 5D). The resting membrane potential of the GFP^+ neurons was around −60 mV and the input resistance was as low as 0.5 GΩ, resembling those of mature neurons (Figure 5E). Over 90% of recorded human neurons fired repetitive APs (Figures 5F and 5G). The F-I curve of human neurons exhibited gradual increases in AP frequency with current injections up to 550 pA (Figure 5H). Similar to those in WT mice, the human iNPC-derived neurons displayed mature membrane properties in the AD brain 6 months after transplantation.

In addition, the grafted human neurons extensively expressed presynaptic markers SYNAPSIN1, SYNAPTOPHYSIN as well as the postsynaptic marker PSD95 (Figure S4B). Abundant green neurites with $PSD95^+$ dots and co-localization of $SYNAPTOPHYSIN^+$ and $GEPHYRIN^+$ dots were detected (Figure 5I). Consistently, human neurons in AD mice received

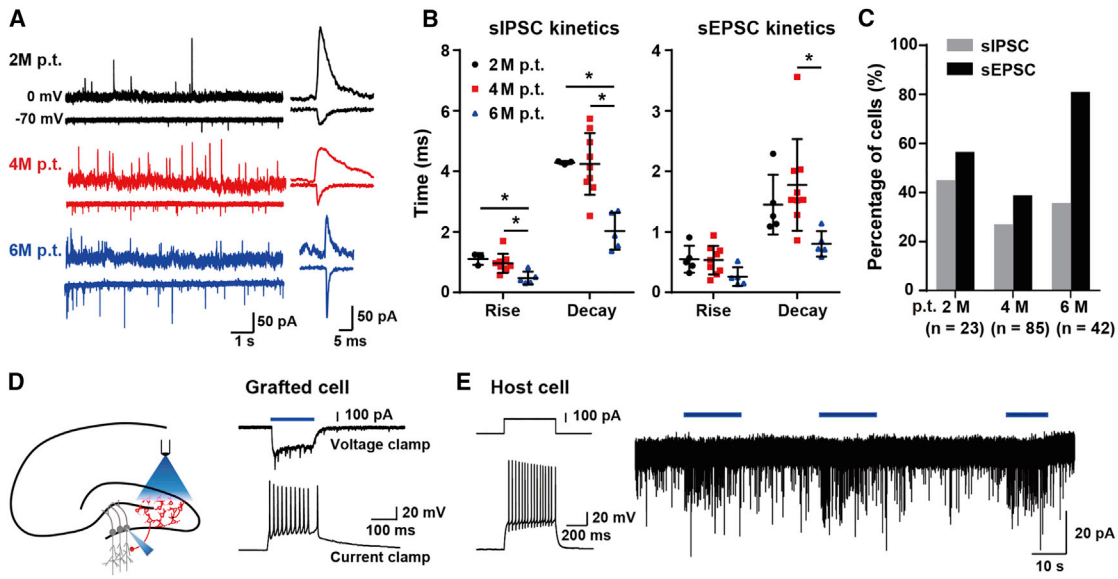

Figure 4. The Functional Integration of Human iNPC-Derived Neurons into Local Synaptic Networks of the Host Hippocampus

(A) Representative traces from human neuronal cells on acute slices from mice brains 2, 4, and 6 M p.t. showing sEPSCs at a holding potential of −70 mV and sIPSCs at 0 mV. Single synaptic events were shown for comparison.

(B) The kinetics of sEPSC and sIPSC from human neuronal cells at 2, 4, and 6 M p.t. Data are represented as scatterplots with mean ± SD. One-way ANOVA followed by Tukey's post-hoc test. *$p < 0.05$.

(C) The percentage of grafted human neuronal cells exhibiting sEPSCs and sIPSCs. Numbers of recorded cells (N) were shown on the graphs.

(D) Left, schematic drawing of the optogenetic experiment on acute slices. Right, blue light activated grafted human cells with ChR2 expression in voltage-clamp and current-clamp mode.

(E) Left, firing pattern of a neighbor host granular cell (GC). Right, light stimulation induced an increase in synaptic inputs in GC recorded in voltage-clamp mode at a holding potential of −70 mV. Sample size: 3 mice for 2 M p.t. and 6 M p.t. group, respectively; 6 mice for 4 M p.t. group; 3 mice for optogenetic assay.

synaptic inputs from neighboring neurons by exhibiting both sEPSCs and sIPSCs (Figures 5J and 5K). Remarkably, the optogenetic assay revealed that the host hippocampal neurons received synaptic inputs when stimulating the grafted human neurons by blue light (Figures 5L and 5M), which directly indicated the synaptic transmission between grafted human neurons and host hippocampal neurons and confirmed the functional integration of human neurons into neural networks of AD mice.

All together, these results demonstrate that the grafted human iNPCs efficiently differentiate into mature neurons forming functionally synaptic connections with hippocampal neurons of the AD mice, suggesting a reinforcement of local neural circuitry upon human iNPC transplantation.

The Grafted Human iNPCs Rescued Cognitive Deficits of AD Mice

It was well documented that long-term potentiation (LTP) was severely impaired in the hippocampus of 5XFAD mice, as in numerous other AD model mice (Crouzin et al., 2013; Kimura and Ohno, 2009). LTP is considered to be an electrophysiological correlate of synaptic plasticity and LTP deficits in AD animals is associated with impaired performance in learning and memory (Chapman et al., 1999; Stephan et al., 2001). Then, we wonder whether the reinforcement in synaptic circuits upon human iNPC transplantation could have an impact on either synaptic or cognitive deficits of AD mice.

To test the synaptic plasticity of AD mice, we measured the LTP in CA3-CA1 pathway of hippocampus on brain slice from $Rag2^{-/-}$/5XFAD mice with grafted human iNPCs 6 months after transplantation together with age-matched $Rag2^{-/-}$/5XFAD littermates without grafted cells, 5XFAD and WT mice (Figure S5A). Grafted GFP^{+} human cells could be observed in the hippocampus of the coronal slices from $Rag2^{-/-}$/5XFAD mice for LTP measurements (Figure S5B). Compared with WT mice, LTP induction by theta-burst stimulation in both 5XFAD and $Rag2^{-/-}$/5XFAD mice was impaired, while $Rag2^{-/-}$/5XFAD mice with grafted human iNPCs showed an increased LTP as high as WT mice (Figure 6A, left). One-way ANOVA comparing the average magnitude of LTP from 35 to 45 min after stimulation confirmed that both 5XFAD and $Rag2^{-/-}$/5XFAD mice

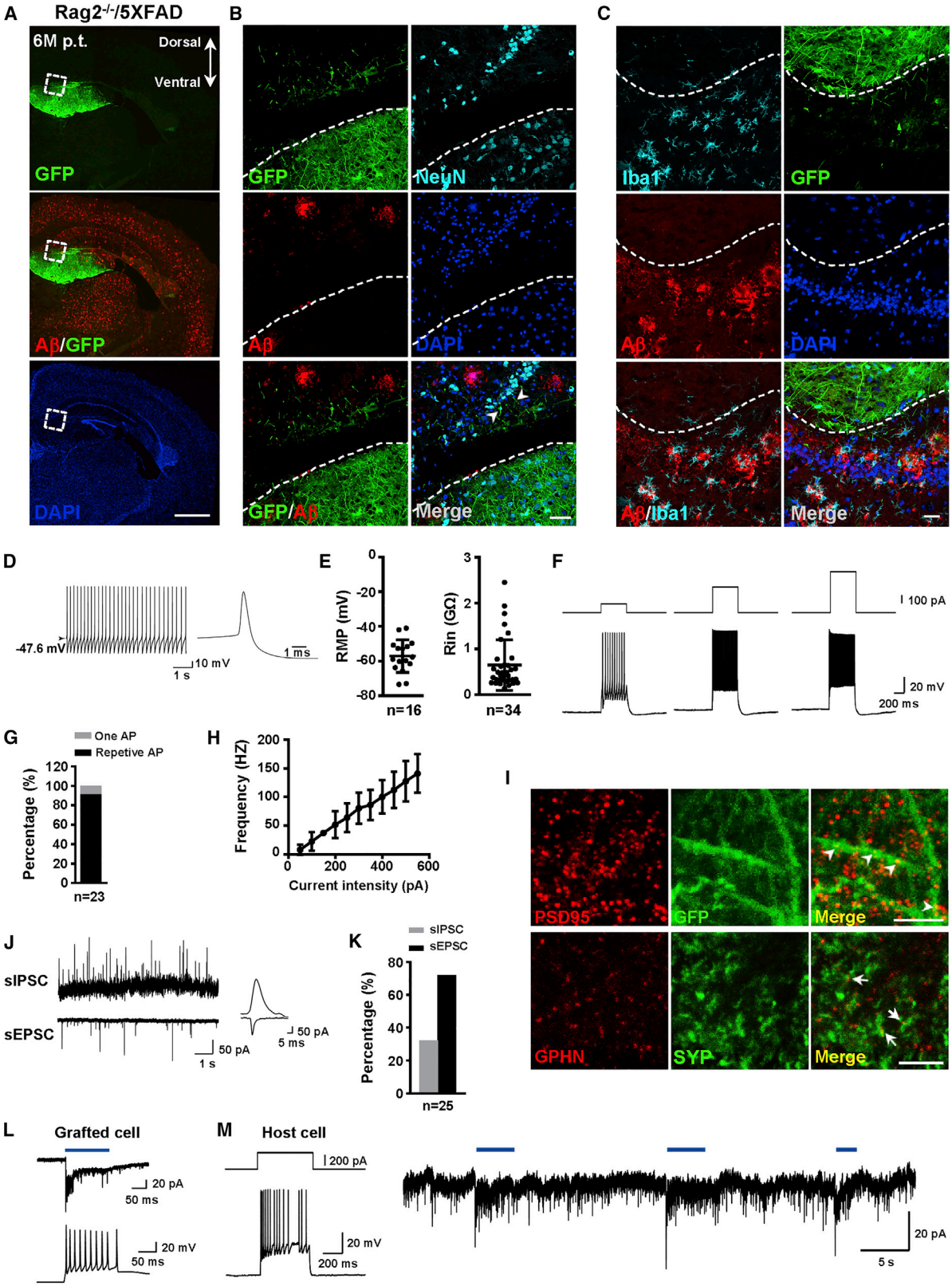

(legend on next page)

had an apparently disrupted LTP, whereas Rag2$^{-/-}$/5XFAD mice with human iNPCs displayed an enhanced LTP comparable with that of WT mice (Figure 6A, right), indicative of improved synaptic plasticity upon transplantation.

The previous studies reported that the secretion of neural trophic factor increased in the brain of AD mice upon transplantation of neural stem cells (Blurton-Jones et al., 2009; Yue et al., 2015). Thus, we measured the secreted brain-derived neurotrophic factor (BDNF) 6 months after transplantation and found that the levels of BDNF in the hippocampus, but not whole brain, were markedly higher in Rag2$^{-/-}$/5XFAD mice with human iNPCs than those without (Figures 6B and S5C), which might contribute to the enhancement of synaptic connections between grafted and host neurons.

We finally assessed the cognitive performance of grafted Rag2$^{-/-}$/5XFAD mice 5 to 6 months after transplantation. Hippocampus-dependent spatial learning and reference memory abilities of WT and AD mice were measured by two behavioral tests, Y-maze spontaneous alternation task and Barnes maze (Figure S5A). In the Y-maze task, the number of arm entries during the test period was not different among groups and all groups of mice actively explored in maze (Figure 6C, left). 5XFAD mice, Rag2$^{-/-}$/5XFAD mice and Rag2$^{-/-}$/5XFAD with vehicle control displayed a significantly decreased alternation frequency compared with WT mice, whereas Rag2$^{-/-}$/5XFAD with human iNPCs exhibited a markedly improved alternation performance reaching the level of WT mice (Figure 6C, right). To further confirm the restored cognitive abilities of AD mice, Barnes maze, a dry-land maze similar to Morris water maze, was performed subsequently. Barnes maze takes advantage of the superior abilities of rodents to find and escape through small holes and avoids strong aversive stimuli, such as water (Barnes, 1979). In Barnes maze test, spatial learning abilities were assessed by latency to reach the target hole during training trials. Grafted Rag2$^{-/-}$/5XFAD mice exhibited gradually and significantly shorter latencies, including both primary and total latency, than AD controls and showed a steady improvement in learning comparable with WT mice (Figure 6D). The probe trials were performed on day 5 to assess spatial memory retention. Grafted Rag2$^{-/-}$/5XFAD mice exhibited decreased primary latency (Figure 6E, left), spent more time searching in the target quadrant (Figure 6E, right) and displayed a recovery in memory abilities comparable with WT mice. In addition, the number of pokes in each hole directly showed the preference of grafted Rag2$^{-/-}$/5XFAD as well as WT mice for the target hole (Figure 6F), reflecting the rescued memory abilities of grafted AD mice.

Together, these results suggest that AD mice exhibited enhancement of synaptic plasticity and evident improvement in cognitive abilities upon transplantation of human iNPCs.

DISCUSSION

In this study, integration-free human iNPCs were generated from peripheral blood cells, which resembled brain NPCs

Figure 5. The Mature and Functional Integration of Human iNPC-Derived Neurons into Local Synaptic Networks of AD Hippocampus

(A) Top, the GFP$^+$ grafted human cells in dentate gyrus on the coronal brain section of Rag2$^{-/-}$/5XFAD mouse 6 M p.t. Bottom, Aβ deposits on the same brain section.

(B) The close-ups of GFP$^+$ grafted human cells shown in (A). Arrow heads indicate that the green long fibers of human neurons in the grafts projected into the host neurons. Dashed lines indicate the borders between human cell grafts and host neurons.

(C) Immunofluorescence analysis of Iba1 in hippocampal region loaded with Aβ plaques and in GFP$^+$ human cell grafts. Dashed lines indicate the borders between human cell grafts and host neurons.

(D) Spontaneous APs recorded in some iNPC-derived neurons. Inset, an expanded AP for clarity.

(E) The resting membrane potential (left) and input resistance (right) of human neuronal cells at 6 M p.t.

(F) AP generation in grafted human neuronal cells in response to step current injection.

(G) Percentage of human neuronal cells with one AP, or repetitive AP at 6 M p.t.

(H) The F-I curve of human neuronal cells at 6 M p.t.

(I) The green neurites from grafted iNPC-derived neurons expressing PSD95 and distributing among host hippocampal neurons at 6 M p.t. (top). Double immunofluorescence analysis of SYP and GPHN (bottom). Arrowheads indicate PSD95 dots in GFP$^+$ human neurites. Arrows indicate co-localization of SYP and GPHN dots.

(J) Representative traces from human neuronal cells at 6 M p.t. showing sEPSCs at a holding potential of −70 mV and sIPSCs at 0 mV.

(K) The percentage of grafted human neuronal cells exhibiting sEPSCs and sIPSCs.

(L) Representative light-induced responses of grafted human cells with ChR2 expression in voltage-clamp (top) and current-clamp mode (bottom).

(M) Left, firing pattern of a neighbor host granular cell (GC). Right, light stimulation induced an increase in synaptic inputs in GC recorded in voltage-clamp mode at a holding potential of −70 mV.

Scale bars, 1 mm (A), 50 μm (B), 25 μm (C), and 5 μm (I). Sample size: 3 mice. Numbers of recorded cells (n) were shown on the graphs in (E), (G), and (K). Data are represented as means ± SD in (E) and (H). Related to Figure S4.

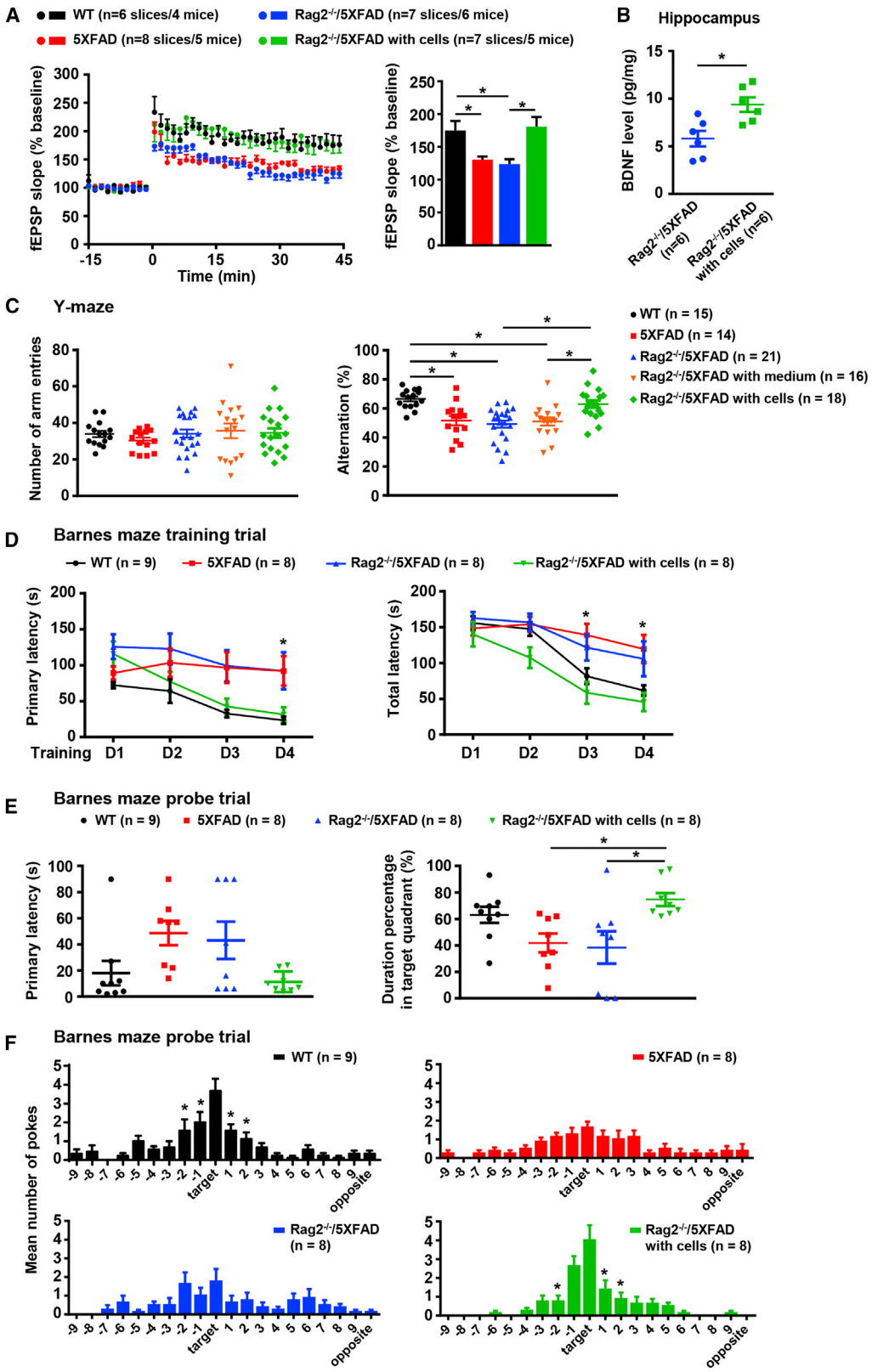

(legend on next page)

both molecularly and physiologically. After transplantation, the human iNPCs differentiated into mature neurons in the hippocampus of adult mice, including AD mice. The functional integration of iNPC-derived neurons into the host synaptic networks contributed to enhance hippocampal plasticity and repair neural circuits of the host brain, which led to improved cognitive abilities of AD mice.

The Possible Application of Human iNPCs to Repair AD Brain

NPCs are multipotent stem cells with limited self-renewal capacity that are found in specific brain regions of mammals (Gage, 2000). Upon stimulation, brain NPCs have the potential to repair neurons lost after disease or injury, but the repairing capacity of NPCs *in vivo* is limited and the mechanisms underlying the activation, proliferation and differentiation of adult NPCs are poorly understood (Gage, 2000). Great efforts have been made *in vitro* to convert human somatic cells into iNPCs that are assumed to have invaluable potential in cell replacement therapies. With the advance of the iPSC technology and a better understanding of the reprogramming process, scientists have started to generate iNPCs from mouse or human fibroblasts via an iPSC intermediate by using transcription factors, such as four core iPSC factors alone or combined with neural lineage-specific factors, such as FoxG1, Zic3, Brn2 (Han et al., 2012; Kumar et al., 2012; Lujan et al., 2012) and with small molecules (Lu et al., 2013; Zhu et al., 2014). In parallel, attempts have been made to direct the reprogramming of human cord blood cells into iNPCs (Castano et al., 2014; Liao et al., 2015). PB MNCs, especially erythroblasts, are more favorable than fibroblasts or cord blood cells for reprogramming due to their easier accessibility, lower mutation burden and suitable epigenetic signature (Dowey et al., 2012). Recently, a study reported the generation of human iNPCs from PB MNCs of one donor using six factors (four iPS factors plus Nanog and Lin28) and two chemicals (Tang et al., 2016). Obviously, the previous studies have primarily focused on developing effective approaches to direct the neural fate conversion of somatic cells. Although the generation of functional iNPCs from human somatic cells has been proposed to be an important step toward regenerative medicine, none of the resulted iNPCs has been tested whether they can function well *in vivo* as *in vitro*.

In this study, we refined the approaches and used episomal vector-based approach to stably generate integration-free human iNPCs from a small volume (as low as 3 mL) of immobilized peripheral blood from several adults (Figures 1A and 1B). The generation of human iNPCs from PB MNCs was easy and rapid and could be in a patient-specific way if necessary. Therefore, iNPCs was more suitable as donor cells for the treatment of neurodegenerative disorders than human mesenchymal stem cells or neural stem cells from fetal brain (Lee et al., 2010; Ager et al., 2015). During iNPC generation, we found that the Yamanaka factors initiated the reprogramming of blood cells, but the four additional chemicals played vital and essential roles in the fully neural fate conversion from PB MNCs to iNPCs (Figure S1A). This observation provides clues to further modify the current approaches for iNPC generation and to uncover the molecular events underlying the switch from PB MNCs to iNPCs. Besides the systematical characterization of the human iNPCs *in vitro* as what previous studies did in general (Figures 1, S1, and S2), we thoroughly investigated the efficacy of human iNPCs *in vivo*. We found that the human iNPCs functioned properly in the host hippocampus of both WT and AD mouse (Figures 2–5). The AD mice benefited from human iNPCs transplantation and displayed improved hippocampus-dependent learning and memory abilities in two behavioral tests, the Y-maze and Barnes maze, suggesting that human iNPCs might be applicable as donor cells for treating AD (Figure 6). Thus, we not only generated the homogeneous, expandable and functional human iNPCs in a more efficient and stable manner, but also evaluated the therapeutic potential of human

Figure 6. Grafted Human iNPCs Enhanced Hippocampal LTP and Rescued Cognitive Deficits of AD Mice

(A) Field potential recording at hippocampus CA3-CA1 pathway showed time course of LTP induced by Tris-buffered saline (left) and average fEPSP amplitudes (% baseline fEPSP) during the last 10 min of recording (right).

(B) The concentration of secreted BDNF by ELISA analyses in hippocampus from Rag2$^{-/-}$/5XFAD mice with and without human iNPCs at 6 M p.t. Student's t test (two-tailed). *p < 0.05.

(C) Y-maze task was performed in five groups of mice, including WT controls, 5XFAD mice, Rag2$^{-/-}$/5XFAD mice, Rag2$^{-/-}$/5XFAD mice with vehicle as sham controls and Rag2$^{-/-}$/5XFAD mice with human iNPCs. Left, the total numbers of arm entries. Right, percentage alternation.

(D) Training trials of Barnes maze revealed that Rag2$^{-/-}$/5XFAD mice with grafted human iNPCs displayed significantly shorter escape latencies than AD mice without iNPCs.

(E) Probe trials of Barnes maze. Rag2$^{-/-}$/5XFAD mice with grafted human iNPCs spent longer time in the target quadrant (right) than AD mice without cells.

(F) Number of pokes in each hole for each group of mice during the probe trial in Barnes maze.

Data are presented as the means ± SEM. One- or two-way ANOVA followed by Tukey's post-hoc test. *p < 0.05. Related to Figure S5.

iNPCs in AD animals. Our results supported the notion that human iNPCs might represent a safer and more reliable material with distinct therapeutic perspective in regenerative medicine for the treatment of AD.

The Reinforcement of Synaptic and Neural Circuits by Grafted Human iNPCs in AD Brain

A better understanding of the neuropathology of AD has led to the realization that a single therapeutic strategy or intervention might not be sufficient for the recovery of cognitive impairments in AD patients. Great efforts have been made by pharmaceutical companies to develop drugs for preventing the deposition or clearing amyloid deposits in AD brain using Aβ vaccine and antibodies, but most therapeutic drugs targeting Aβ in clinic or under development have failed to rescue or slow AD symptoms. Deficits in neural circuit stabilization or integrity and synaptic plasticity at early stages of AD directly lead to cognitive dysfunction (Palop and Mucke, 2010; Selkoe, 2002). It is thought that restoring the integrity of synaptic and neural circuit might provide new directions for memory recovery in AD (Canter et al., 2016). Because of the tremendous therapeutic potential, different types of neural stem cells have been tested in AD animals for the possible therapeutic use in AD over the last decade (Ager et al., 2015; Lee et al., 2010; Liu et al., 2013; Moghadam et al., 2009). These studies have consistently reported that grafted NSCs improved to some degree the cognitive performances of AD animal models, but none of these studies have interrogated the changes in synaptic and neural circuits upon transplantation. The only exception published recently has failed to demonstrate the safety and efficacy of fetal brain-derived human NSCs (STEMCELL; HuCNS-SCs) in the Rag-5XFAD immune-deficient mouse 5 months after transplantation (Marsh et al., 2017). Thus, how the NSCs rescued the cognitive deficits of AD mouse or even whether the NSCs could be suitable for replacement therapy remain somewhat ambiguous.

In our previous study, we transplanted mouse ESC-derived BFCN progenitors into the basal forebrain of AD model mice. Two months after transplantation, the grafted BFCN progenitors differentiated into functional cholinergic neurons and the AD mice exhibited improvements in learning and memory performances (Yue et al., 2015). Further investigation showed that the grafted BFCNs expressed postsynaptic potentials and formed synapses with host neurons, which might contribute to ameliorate cognitive deficits of AD mice (Yue et al., 2015). To test different types of donor cells in different brain regions of AD mice, we performed a follow-up study here to systematically evaluate the safety of human iNPCs and address the potential of human iNPCs in repairing the disrupted synaptic networks of AD mice. First, the human iNPCs were transplanted into the hippocampus of WT and AD mice and evaluated for both short-term (1 and 2 months) and long-term (4, 6, and 12 months) observations. The Oct4 expression could not be detected among human iNPCs (Figure 1), which is critical for the safety concerns of transplantation. In addition, the human iNPCs are a homogeneous population (Figures 1, S1, and S2). The neural progenitors from ESCs or iPSCs were usually mixed and were hardly generated in a controlled way owing to the nonsynchronous differentiation of pluripotent stem cells (Liu et al., 2013; Moghadam et al., 2009). The grafted human iNPCs stopped proliferation *in vivo* and rapidly underwent terminal differentiation to give rise to mature neurons (Figures 2 and 5). No detectable graft overgrowth in the hippocampus or ectopic cell clusters in other regions of brain were detected at all the time points measured (39 WT mice and 22 AD mice) (Figures 2, 5, and S3), suggesting that iNPCs could safely modify the long-term progression of AD. Second, we confirmed the functional integration of grafted human iNPC-derived neurons, which in turn strengthened the impaired synaptic networks and reinforced the neural circuits in the AD brains (Figures 3, 4, 5, and 6). The human iNPC grafts were not invaded by Aβ plaques and neuroinflammation (Figure 5). Then, the iNPC-derived neurons had remained healthy for a long period of time (at least 12 months) in the hippocampus of AD mice (Figure 5). The grafted human neurons displayed high synaptic activities and received synaptic inputs from neighboring cells and functioned properly *in vivo* (Figures 4 and 5). In addition, the optogenetic approach in WT and AD mice revealed the graft-to-host synaptic transmission between human and murine neurons, directly elucidating that grafted human neurons functionally integrated into the synaptic circuitry (Figure 5). Consequently, grafted AD mice exhibited increased LTP and enhanced synaptic plasticity (Figure 6), suggesting that the integration of human neurons could repair the synaptic dysfunction of AD brain. These observations partially explained why grafted NPCs could alleviate the cognitive deficits of AD mice.

Unlike Parkinson's disease, the AD brain displayed global neuron loss. Thus, a single-pronged transplantation approach by using one type of donor cells to the treatment of AD may be insufficient. For that matter, the cell replacement for AD might need simultaneous transplantation of multiple types of neural cells and even with astrocytes into different brain regions, particular the cognition-relevant brain regions. So far, we had transplanted the BFCN progenitors into basal forebrain (Yue et al., 2015) and iNPCs, the glutamatergic neuron progenitors, into hippocampus of AD mice, respectively. Both types of grafted neural progenitors gave rise to mature and functional neurons that integrated into the host neural circuits and reinforced the synaptic networks. These attempts indicated that one

type of grafted neural cells could target one brain region and repair the dysfunction of local neural networks of AD brain. Therefore, we deduced that various grafted NPCs could simultaneously repair multiple brain regions and ultimately alleviated the cognitive deficits of AD patients. The future study will address the establishment of transplantation strategies combining different NPCs in AD mouse and test whether different types of grafted neurons could function synergistically and improve the cognitive abilities of AD mouse better.

Together, our findings demonstrate that iNPCs derived from human peripheral blood differentiate into mature neurons in the hippocampus of host mice. These grafted human neurons functionally integrate into the host hippocampus, increase the synaptic connectivity and synaptic plasticity, reinforce the local neural circuit integrity and finally lead to the cognitive recovery of AD mice. Our study provides evidence supporting a possible therapeutic target for stem cell-based therapies, suggesting that iNPCs derived from somatic cells of individuals could be developed to restore the synaptic failures and functional impairments of AD.

EXPERIMENTAL PROCEDURES

Isolation and Expansion of Human Adult PB MNCs

The use of human adult peripheral blood was approved by the Biomedical Research Ethics Committee, SIBS, CAS, and Ruijin Hospital Ethics Committee, Shanghai JiaoTong University School of Medicine, with written informed consent from the donors. Three participants were recruited in the study and designated as donor 1, 2, and 3, respectively. Isolation and expansion of PB MNCs was performed as described previously (Dowey et al., 2012). The additional details are included in the Supplemental Experimental Procedures.

Generation of iNPCs from Human Adult PB MNCs by Episomal Vector Transfection

The oriP/EBNA1-based episomal vectors EV SFFV-OCT4-2A-SOX2 (SFFV-OS), EV SFFV-MYC-2A-KLF4 (SFFV-MK), and EV SFFV-BCL-XL have been described previously (Su et al., 2013). The process for human iNPC generation is schematically summarized in Figure 1A. Two million PB MNCs were nucleofected with a mixture of the episomal vectors following the Amaxa 4D-Nucleofector Protocols for Unstimulated Human CD34$^+$ Cells (Lonza). Subsequent steps in iNPC generation are detailed in the Supplemental Experimental Procedures.

Cell Transplantation

The animal experiments were performed following protocols approved by the Animal Ethics Committee of the Shanghai Institutes for Biological Sciences. The immunodeficient Foxn1$^{-/-}$ mice were purchased from Shanghai SLAC Laboratory Animal Company (Shanghai, China). The AD model mice 5XFAD (Jackson Laboratory, no. 006554) was purchased from Jackson Laboratory. Rag2$^{-/-}$/5XFAD immunodeficient AD model mice were generated by crossing 5XFAD mice with Rag2$^{-/-}$ mice (a gift from Dr. Lijian Hui, SIBCB, China). Male mice were used in the study. GFP$^+$ or ChR2-mCherry$^+$ human iNPCs at passage 15 were targeted to the hippocampus DG region following coordinates relative to bregma: AP, −1.06 mm; ML, ±1.0 mm; DV, −2.5 mm. The cell transplantation was performed in immunodeficient Foxn1$^{-/-}$ mice at 2 months of age and Rag2$^{-/-}$/5XFAD mice at 4 months of age. Details of the cell transplantation procedure are included in the Supplemental Experimental Procedures.

Electrophysiological Recording

Whole-cell patch-clamp recording was performed in human iNPC-derived neurons on differentiating day 50 (*in vitro*) and in EGFP$^+$ or mCherry$^+$ human iNPC-derived neurons in the coronal brain slices of immunodeficient mice (*in vivo*). The whole-cell recordings were performed with a MultiClamp 700B (Molecular Devices). The cultured cells were patched as described previously (Yue et al., 2015). The additional details of acute brain slices preparation, electrophysiological recording, optogenetic experiment and field potential recording are included in the Supplemental Experimental Procedures.

Behavioral Tests (Y-Maze and Barnes Maze)

The behavioral tests were performed in Rag2$^{-/-}$/5XFAD with or without grafted human iNPCs at 9–10 months of age (5–6 months after transplantation) and age-matched WT and 5XFAD mice. Y-maze spontaneous alternation task was performed as described previously (Ohno et al., 2006). Barnes maze behavior test was performed as described previously (Sunyer et al., 2007). The additional details are included in the Supplemental Experimental Procedures.

Statistical Analysis

All statistical analyses were performed in GraphPad Prism software (GraphPad 7.0). Cell counting and electrophysiological data were presented as mean ± SD, while BDNF ELISA, behavior test, and LTP data were presented as mean ± SEM. Student's t test (two-tailed) was performed for statistical analysis between two groups. One- or two-way ANOVA with Tukey's multiple comparison post-hoc test was used when three or more groups were compared. Sample size (n) values were provided in the relevant text, figures, and figure legends. The statistical analyses were obtained from three independent experiments. Statistical significance was set at $^*p < 0.05$.

ACCESSION NUMBERS

All RNA sequencing data are available at the GEO under accession number GSE107806.

SUPPLEMENTAL INFORMATION

Supplemental Information can be found online at https://doi.org/10.1016/j.stemcr.2019.10.012.

AUTHOR CONTRIBUTIONS

N.J., X.Zhang, and C.Y. initiated the study. T.Z. and C.Y. designed and performed the experiments. W.K. and Y.S. performed

electrophysiological experiments. X.Zhou, Y.D., and X.C. performed behavioral test and LTP measurements. Y.Q. contributed mouse strain generation and performed cell transplantation experiments. S.F., R.W., G.C., R.T., and W.G. performed other experiments. N.J., C.Y., Y.S., and T.Z. conceived the study and interpreted results. C.Y. and Y.S. wrote the manuscript. N.J. supervised the study.

ACKNOWLEDGMENTS

This work was supported in part by the "Strategic Priority Research Program" of the Chinese Academy of Sciences, grant no. (XDA16020501, XDA16020404), National Key Basic Research and Development Program of China (2018YFA0108000, 2018YFA0107200, 2017YFA0102700, 2015CB964500, 2014CB964804), National Natural Science Foundation of China (81671224, 31661143042, 91519314, 31630043, 31601185, 31571513, 31430058, 31471077). We are grateful to T. Li, D.M. Lai at Shanghai Jiao Tong University School of Medicine for their supporting in karyotype analysis. We would like to thank Dr. Francois Guillemot (The Francis Crick Institute, London) and Dr. Harold Gainer (NIH, Maryland) for their critical reading of the manuscript.

Received: January 16, 2019
Revised: October 21, 2019
Accepted: October 23, 2019
Published: November 21, 2019

REFERENCES

Ager, R.R., Davis, J.L., Agazaryan, A., Benavente, F., Poon, W.W., LaFerla, F.M., and Blurton-Jones, M. (2015). Human neural stem cells improve cognition and promote synaptic growth in two complementary transgenic models of Alzheimer's disease and neuronal loss. Hippocampus *25*, 813–826.

Barnes, C.A. (1979). Memory deficits associated with senescence: a neurophysiological and behavioral study in the rat. J. Comp. Physiol. Psychol. *93*, 74–104.

Blurton-Jones, M., Kitazawa, M., Martinez-Coria, H., Castello, N.A., Muller, F.J., Loring, J.F., Yamasaki, T.R., Poon, W.W., Green, K.N., and LaFerla, F.M. (2009). Neural stem cells improve cognition via BDNF in a transgenic model of Alzheimer disease. Proc. Natl. Acad. Sci. U S A *106*, 13594–13599.

Brand, A.H., and Livesey, F.J. (2011). Neural stem cell biology in vertebrates and invertebrates: more alike than different? Neuron *70*, 719–729.

Cacabelos, R. (2018). Have there been improvements in Alzheimer's disease drug discovery over the past 5 years? Expert Opin. Drug Discov. *13*, 523–538.

Canter, R.G., Penney, J., and Tsai, L.H. (2016). The road to restoring neural circuits for the treatment of Alzheimer's disease. Nature *539*, 187–196.

Castano, J., Menendez, P., Bruzos-Cidon, C., Straccia, M., Sousa, A., Zabaleta, L., Vazquez, N., Zubiarrain, A., Sonntag, K.C., Ugedo, L., et al. (2014). Fast and efficient neural conversion of human hematopoietic cells. Stem Cell Reports *3*, 1118–1131.

Chapman, P.F., White, G.L., Jones, M.W., Cooper-Blacketer, D., Marshall, V.J., Irizarry, M., Younkin, L., Good, M.A., Bliss, T.V., Hyman, B.T., et al. (1999). Impaired synaptic plasticity and learning in aged amyloid precursor protein transgenic mice. Nat. Neurosci. *2*, 271–276.

Crouzin, N., Baranger, K., Cavalier, M., Marchalant, Y., Cohen-Solal, C., Roman, F.S., Khrestchatisky, M., Rivera, S., Feron, F., and Vignes, M. (2013). Area-specific alterations of synaptic plasticity in the 5XFAD mouse model of Alzheimer's disease: dissociation between somatosensory cortex and hippocampus. PLoS One *8*, e74667.

Davies, C.A., Mann, D.M., Sumpter, P.Q., and Yates, P.O. (1987). A quantitative morphometric analysis of the neuronal and synaptic content of the frontal and temporal cortex in patients with Alzheimer's disease. J. Neurol. Sci. *78*, 151–164.

Doody, R.S., Thomas, R.G., Farlow, M., Iwatsubo, T., Vellas, B., Joffe, S., Kieburtz, K., Raman, R., Sun, X., Aisen, P.S., et al. (2014). Phase 3 trials of solanezumab for mild-to-moderate Alzheimer's disease. N. Engl. J. Med. *370*, 311–321.

Dowey, S.N., Huang, X., Chou, B.K., Ye, Z., and Cheng, L. (2012). Generation of integration-free human induced pluripotent stem cells from postnatal blood mononuclear cells by plasmid vector expression. Nat. Protoc. *7*, 2013–2021.

Gage, F.H. (2000). Mammalian neural stem cells. Science *287*, 1433–1438.

Han, D.W., Tapia, N., Hermann, A., Hemmer, K., Hoing, S., Arauzo-Bravo, M.J., Zaehres, H., Wu, G., Frank, S., Moritz, S., et al. (2012). Direct reprogramming of fibroblasts into neural stem cells by defined factors. Cell Stem Cell *10*, 465–472.

Hardy, J., and Selkoe, D.J. (2002). The amyloid hypothesis of Alzheimer's disease: progress and problems on the road to therapeutics. Science *297*, 353–356.

Hurd, M.D., Martorell, P., Delavande, A., Mullen, K.J., and Langa, K.M. (2013). Monetary costs of dementia in the United States. N. Engl. J. Med. *368*, 1326–1334.

Kimura, R., and Ohno, M. (2009). Impairments in remote memory stabilization precede hippocampal synaptic and cognitive failures in 5XFAD Alzheimer mouse model. Neurobiol. Dis. *33*, 229–235.

Kumar, A., Declercq, J., Eggermont, K., Agirre, X., Prosper, F., and Verfaillie, C.M. (2012). Zic3 induces conversion of human fibroblasts to stable neural progenitor-like cells. J. Mol. Cell Biol. *4*, 252–255.

Lee, H.J., Lee, J.K., Lee, H., Shin, J.W., Carter, J.E., Sakamoto, T., Jin, H.K., and Bae, J.S. (2010). The therapeutic potential of human umbilical cord blood-derived mesenchymal stem cells in Alzheimer's disease. Neurosci. Lett. *481*, 30–35.

Liao, W., Huang, N., Yu, J., Jares, A., Yang, J., Zieve, G., Avila, C., Jiang, X., Zhang, X.B., and Ma, Y. (2015). Direct conversion of cord blood CD34+ cells into neural stem cells by OCT4. Stem Cell Transl. Med. *4*, 755–763.

Liu, Y., Weick, J.P., Liu, H., Krencik, R., Zhang, X., Ma, L., Zhou, G.M., Ayala, M., and Zhang, S.C. (2013). Medial ganglionic eminence-like cells derived from human embryonic stem cells correct learning and memory deficits. Nat. Biotechnol. *31*, 440–447.

Lu, J., Liu, H., Huang, C.T., Chen, H., Du, Z., Liu, Y., Sherafat, M.A., and Zhang, S.C. (2013). Generation of integration-free and region-specific neural progenitors from primate fibroblasts. Cell Rep. *3*, 1580–1591.

Lujan, E., Chanda, S., Ahlenius, H., Sudhof, T.C., and Wernig, M. (2012). Direct conversion of mouse fibroblasts to self-renewing, tripotent neural precursor cells. Proc. Natl. Acad. Sci. U S A *109*, 2527–2532.

Marsh, S.E., Yeung, S.T., Torres, M., Lau, L., Davis, J.L., Monuki, E.S., Poon, W.W., and Blurton-Jones, M. (2017). HuCNS-sc human NSCs fail to differentiate, form ectopic clusters, and provide no cognitive benefits in a transgenic model of Alzheimer's disease. Stem Cell Reports *8*, 235–248.

Moghadam, F.H., Alaie, H., Karbalaie, K., Tanhaei, S., Nasr Esfahani, M.H., and Baharvand, H. (2009). Transplantation of primed or unprimed mouse embryonic stem cell-derived neural precursor cells improves cognitive function in Alzheimerian rats. Differentiation *78*, 59–68.

Ohno, M., Chang, L., Tseng, W., Oakley, H., Citron, M., Klein, W.L., Vassar, R., and Disterhoft, J.F. (2006). Temporal memory deficits in Alzheimer's mouse models: rescue by genetic deletion of BACE1. Eur. J. Neurosci. *23*, 251–260.

Palop, J.J., and Mucke, L. (2010). Amyloid-beta-induced neuronal dysfunction in Alzheimer's disease: from synapses toward neural networks. Nat. Neurosci. *13*, 812–818.

Selkoe, D.J. (2002). Alzheimer's disease is a synaptic failure. Science *298*, 789–791.

Stephan, A., Laroche, S., and Davis, S. (2001). Generation of aggregated beta-amyloid in the rat hippocampus impairs synaptic transmission and plasticity and causes memory deficits. J. Neurosci. *21*, 5703–5714.

Su, R.J., Baylink, D.J., Neises, A., Kiroyan, J.B., Meng, X., Payne, K.J., Tschudy-Seney, B., Duan, Y., Appleby, N., Kearns-Jonker, M., et al. (2013). Efficient generation of integration-free iPS cells from human adult peripheral blood using BCL-XL together with Yamanaka factors. PLoS One *8*, e64496.

Sunyer, B., Patil, S., Höger, H., and Lubec, G. (2007). Barnes maze, a useful task to assess spatial reference memory in the mice. Protoc. Exch. https://doi.org/10.1038/nprot.2007.390.

Tang, X., Wang, S., Bai, Y., Wu, J., Fu, L., Li, M., Xu, Q., Xu, Z.Q., Alex Zhang, Y., and Chen, Z. (2016). Conversion of adult human peripheral blood mononuclear cells into induced neural stem cell by using episomal vectors. Stem Cell Res. *16*, 236–242.

van de Leemput, J., Boles, N.C., Kiehl, T.R., Corneo, B., Lederman, P., Menon, V., Lee, C., Martinez, R.A., Levi, B.P., Thompson, C.L., et al. (2014). CORTECON: a temporal transcriptome analysis of in vitro human cerebral cortex development from human embryonic stem cells. Neuron *83*, 51–68.

Yue, W., Li, Y., Zhang, T., Jiang, M., Qian, Y., Zhang, M., Sheng, N., Feng, S., Tang, K., Yu, X., et al. (2015). ESC-derived basal forebrain cholinergic neurons ameliorate the cognitive symptoms associated with Alzheimer's disease in mouse models. Stem Cell Reports *5*, 776–790.

Zhu, S., Ambasudhan, R., Sun, W., Kim, H.J., Talantova, M., Wang, X., Zhang, M., Zhang, Y., Laurent, T., Parker, J., et al. (2014). Small molecules enable OCT4-mediated direct reprogramming into expandable human neural stem cells. Cell Res. *24*, 126–129.

Stem Cell Reports, Volume *13*

Supplemental Information

Human Neural Stem Cells Reinforce Hippocampal Synaptic Network and Rescue Cognitive Deficits in a Mouse Model of Alzheimer's Disease

Ting Zhang, Wei Ke, Xuan Zhou, Yun Qian, Su Feng, Ran Wang, Guizhong Cui, Ran Tao, Wenke Guo, Yanhong Duan, Xiaobing Zhang, Xiaohua Cao, Yousheng Shu, Chunmei Yue, and Naihe Jing

Figure S1. Related to Figure 1

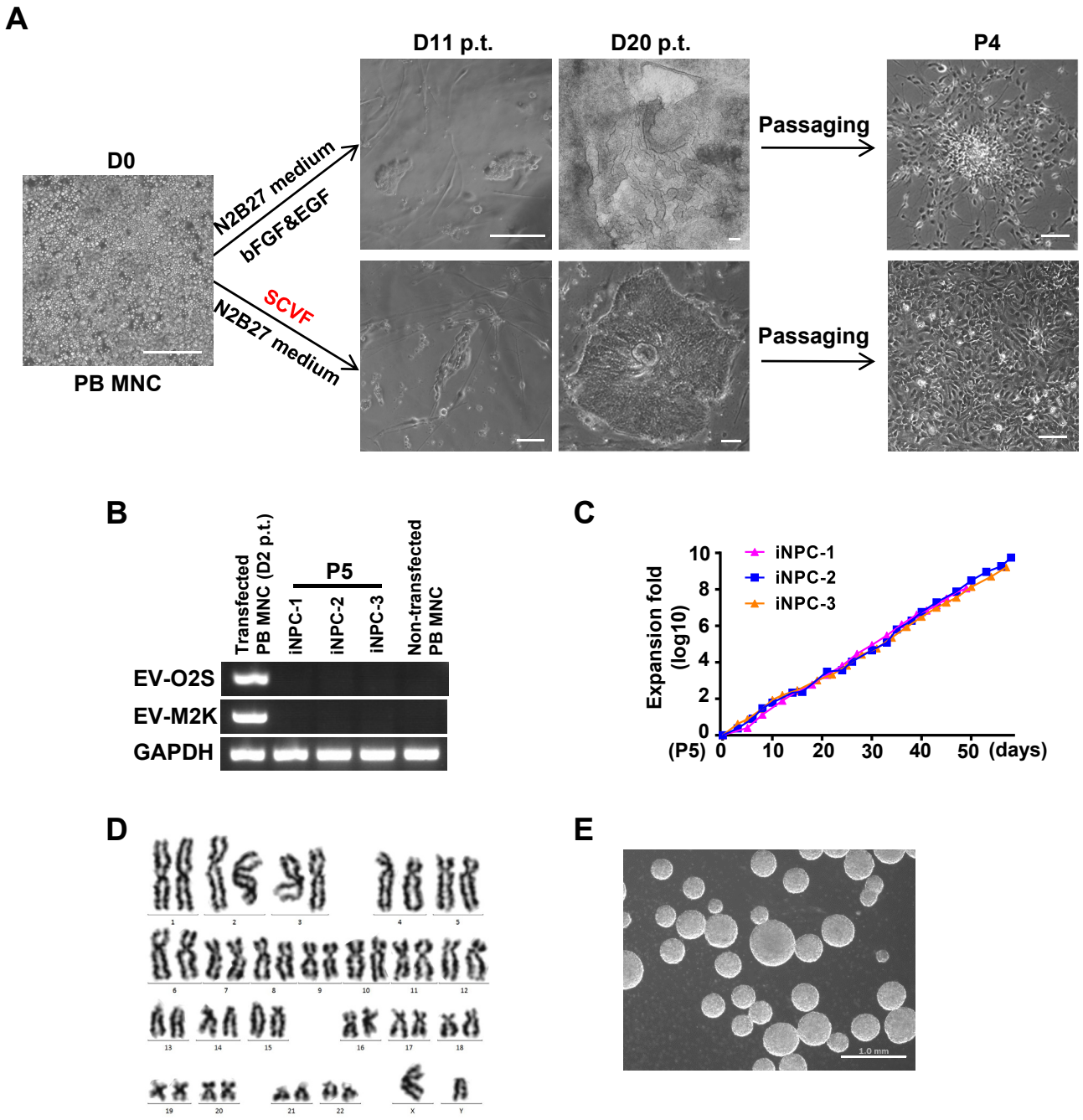

Figure S1. Direct reprogramming of peripheral blood cells into human iNPCs

A. Morphology of early human iNPC clusters at day 11 and 20 after transfection, respectively, and colonies at passage 4 generated without 4 chemicals in N2B27 containing bFGF and EGF, or with 4 chemicals in N2B27 only.

B. PCR analysis of the episomal vector-harboring iPS genes in PB MNCs 2 days after transfection, in three human iNPC lines at passage 5 and in PB MNCs without factor transfection.

C. Growth-curve showing the stable maintenance of human iNPCs up to 25 passages.

D. The karyotype analysis of human iNPCs at passage 25.

E. Neurospheres formed by human iNPCs at passage 15.

Scale bars, 200 μm (A) and 1 mm (E).

Figure S2. Related to Figure 1

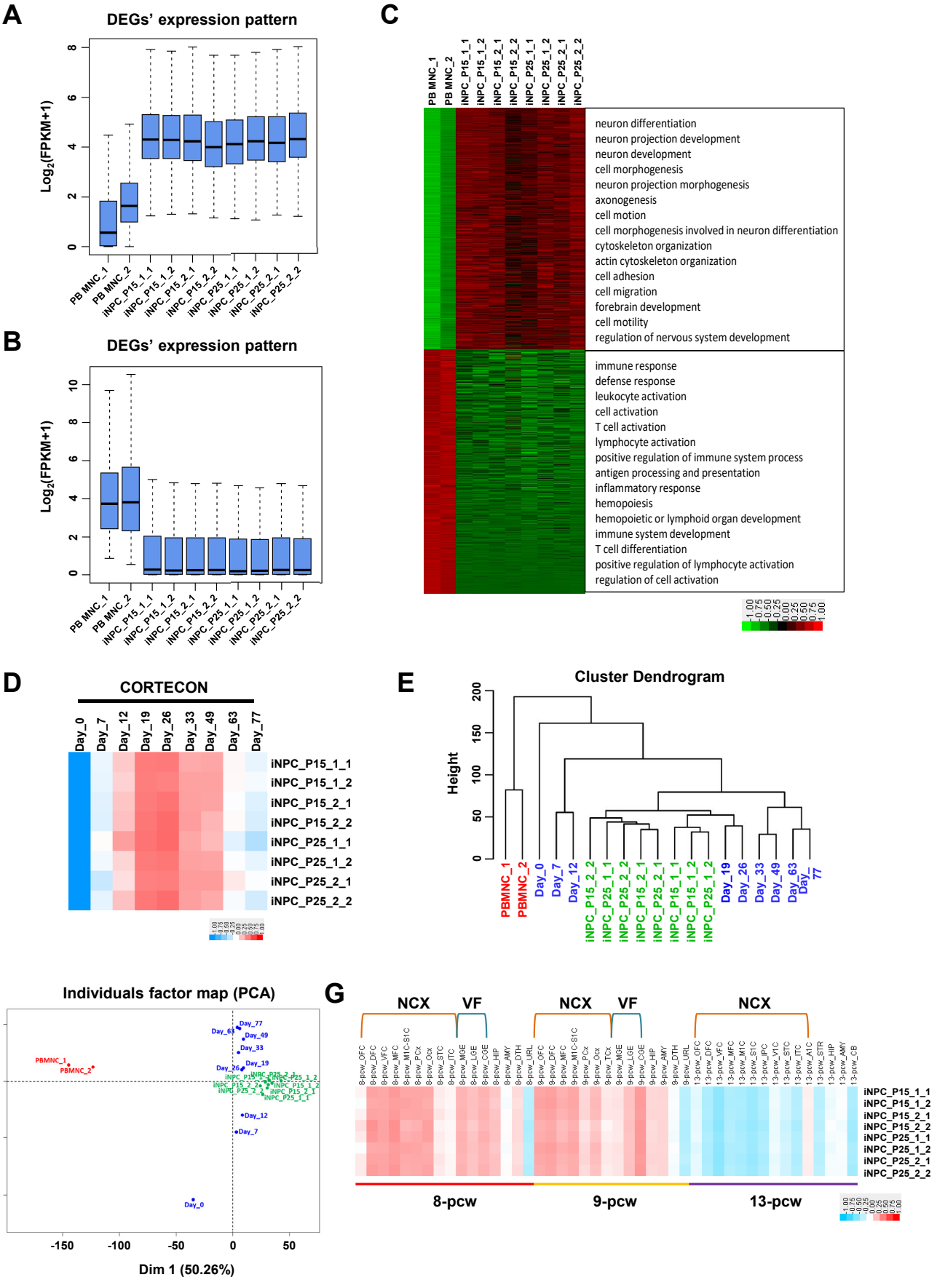

Figure S2. Whole transcriptome profiling of human iNPCs

A. The expression pattern of top 1000 upregulated differential expressed genes (DEGs) from RNA sequencing of PB MNCs from two individuals, and two PB MNC-derived iNPCs at passage 15 and 25 with two representative lines, respectively.

B. The expression pattern of top 1000 downregulated DEGs from RNA sequencing of PB MNCs from two individuals, and two PB MNC-derived iNPCs at passage 15 and 25 with two representative lines, respectively.

C. Heat map based on bulk RNA-sequencing data demonstrating global gene expression pattern of PB MNCs from two individuals, and two PB MNC-derived iNPCs at passage 15 and 25 with two representative lines, respectively. The enrichments of biological relevance in right panel highlighted by Gene Ontology (GO) analysis. Red and green colors represent higher and lower gene expression levels, respectively.

D. Comparative analysis of whole transcriptome of human iNPCs to a published temporal transcriptome dataset of hESC-derived NPCs with prefrontal cortex identity.

E. Hierarchical cluster analysis of the gene expression profiles of PB MNCs and human iNPCs shown in 1F, and a published temporal transcriptome dataset of hESC-derived NPCs.

F. Scatter plot analysis of the global gene expression profiles of human iNSCs at passage 15 and 25 versus the PB MNCs and hESC-derived NPCs.

G. Comparative analysis of whole transcriptome of human iNPCs to database from BrainSpan Atlas of the Developing Human Brain.

Figure S3. Related to Figure 2

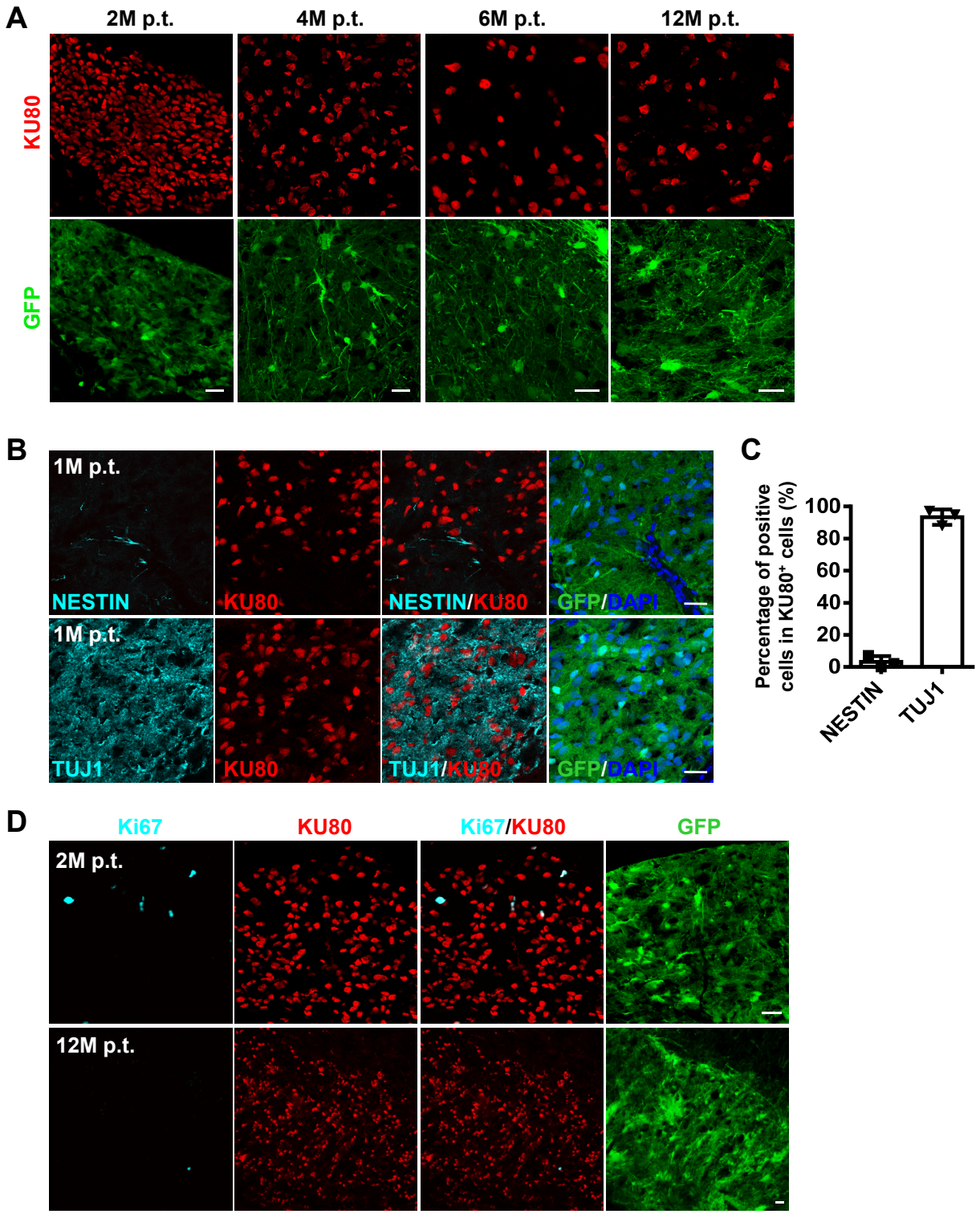

Figure S3. Human iNPCs gave rise to neurons and astrocytes in mice hippocampus after transplantation

A. Immunofluorescence analysis of $KU80^+$ among GFP^+ grafted human cells at 2, 4, 6 and 12 months post transplantation (p.t.).
B. Immunofluorescence analysis of NESTIN (top) or TUJ1(bottom) expression among $KU80^+$ human cells at 1 month p.t.
C. Quantification of the results shown in B. Note the small percentage of $NESTIN^+$ neural progenitor cells among $KU80^+$ human cells.
D. Immunofluorescence analysis of Ki67 expression among $KU80^+$ human cells at 2 and 12 months p.t.

Scale bars, 25 μm (A, B and D). n = 3 mice per time point. Data are represented as scatter plots with mean ± SD.

Figure S4. Related to Figure 5

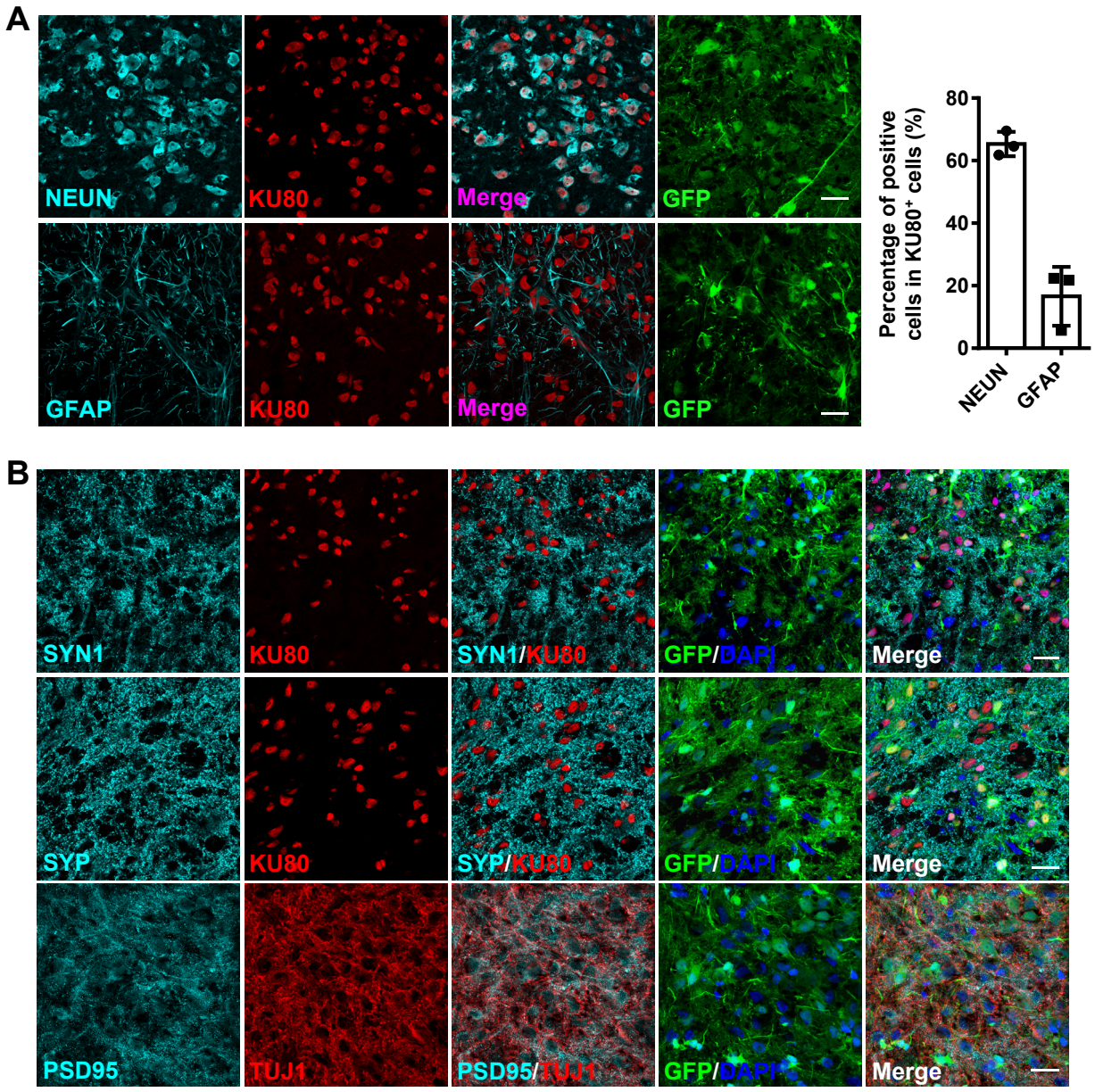

Figure S4. Differentiation of human iNPCs in hippocampus of AD mice after transplantation

A. Immunofluorescence analysis of NEUN or GFAP expression among KU80^{+} human cells in the hippocampus of Rag2$^{-/-}$/AD mice at 4 months p.t. (left panel) and the quantitative analysis shown in the right panel. n = 3 mice. Data are represented as scatter plots with mean ± SD.

B. Double immunofluorescence analysis of presynaptic markers SYNAPSIN1 or SYNAPTOPHYSIN with KU80 expression as well as postsynaptic marker PSD95 with TUJ1 expression among GFP^{+} human cells in the hippocampus of Rag2$^{-/-}$/AD mice at 4 months p.t.

Scale bars, 25 μm (A, B).

Figure S5. Related to Figure 6

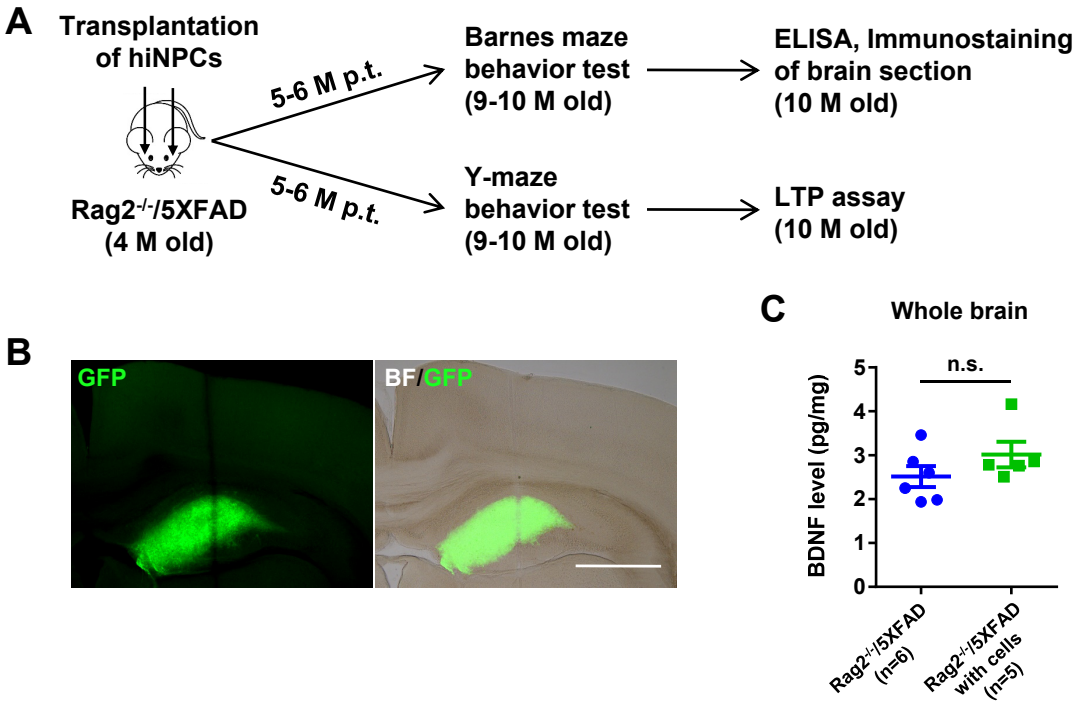

Figure S5. The grafted green human iNPCs in hippocampus of host mice

A. Schematic representation of timeline for human iNPCs transplantation and subsequent measurements in AD mice.

B. The GFP^+ human cells in hippocampus on the coronal brain slice from transplanted mice at 6 months post transplantation and after LTP measurement. Scale bar, 1 mm.

The concentration of secreted BDNF in whole brain of $Rag2^{-/-}$/5XFAD with and without human iNPCs at 6 months p.t. Data are presented as scatter plots with mean ± SEM. Student's t test (two-tailed), P=0.212.

Table S1. Primary antibody list.

Primary antibodies					
Name	**Host**	**Company**	**Cat.No.**	**Dillution**	**RRID**
PAX6	Rabbit	Chemicon	AB2237	1:200	AB_1587367
SOX1	Rabbit	Self-produced	/	1:200	/
SOX2	Rabbit	Abcam	ab59776	1:200	AB_945584
NESTIN	Rabbit	Self-produced	/	1:200	/
Ki67	Rabbit	Abcam	ab16667	1:50	AB_302459
FABP7	Rabbit	Abclonal	A3246	1:50	/
NANOG	Goat	R&D	AF1997	1:200	AB_355097
OCT4	Mouse	Santa cruz	SC-5279	1:200	AB_628051
TUJ1	Mouse	Biolegend	MMS-435P	1:500	AB_2313773
TUJ1	Rabbit	Biolegend	MRB-435P	1:500	AB_663339
MAP2	Mouse	Sigma	M4403	1:200	AB_477193
NEUN	Rabbit	Millipore	ABN78	1:200	AB_10807945
GFAP	Rabbit	Abcam	ab16997	1:200	AB_443592
O4	Mouse (IgM)	Chemicon	MAB345	1:50	AB_94872
TBR1	Rabbit	Abcam	ab31940	1:100	AB_2200219
VGLUT1	Rabbit	SYSY	135302	1:200	/
GAD67	Mouse	Millipore	MAB5406	1:200	AB_2278725
Tyrosine Hydroxylase (TH)	Rabbit	Millipore	AB152	1:500	AB_390204
ChAT	Goat	Millipore	AB144P	1:100	AB_2079751
KU80 (STEM101)	Mouse	Takara	Y40400	1:100	/
Synapsin 1 (SYN1)	Rabbit	Millipore	574777	1:200	AB_2200124
Synaptophysin (SYP)	Rabbit	Abcam	ab32127	1:200	AB_2286949
Synaptophysin (SYP)	Mouse	SYSY	101011	1:200	AB_887824
Gephyrin (GPHN)	Mouse	SYSY	147011	1:500	AB_887717
PSD95	Rabbit	Abcam	ab18258	1:1000	AB_444362
6E10	Mouse	Covance	SIG-39300	1:200	AB_662803
Iba1	Rabbit	Wako	1919741	1:1000	AB_2665520

SUPPLEMENTAL EXPERIMENTAL PROCEDURES

Isolation and expansion of human adult peripheral blood mononuclear cells (PB MNC)

The use of human adult peripheral blood was approved by the Biomedical Research Ethics Committee, SIBS, CAS, and Ruijin Hospital Ethics Committee, Shanghai JiaoTong University School of Medicine, with written informed consent from the donors. 3 participants were recruited in the study. They were 30-, 61- and 56-year old healthy male adults, and designated as donor 1, 2 and 3, respectively. Isolation and expansion of peripheral blood mononuclear cells (PB MNCs) was performed as previously described (Dowey et al., 2012). Briefly, 3-8 ml of adult peripheral blood was collected, and mononuclear cells (MNCs) were isolated using Ficoll-Paque Premium (Sigma) by density gradient centrifugation. The MNCs were then cultured for 8 to 12 days in MNC medium (IMDM: Ham's F12 (1: 1) supplemented with 1% ITS-X, 1% chemically defined lipid concentrate, 1×Glutamax, 50 μg/ml L-ascorbic acid (Sigma), 5 mg/ml BSA (Sigma), 200 μM 1-thioglycerol (Sigma), 100 ng/ml SCF (PeproTech), 10 ng/ml IL-3 (PeproTech), 2 U/ml EPO (R&D system), 40 ng/ml IGF-1 (PeproTech), 1 μM dexamethasone (MP Biomedicals) and 100 μg/ml holo-transferrin (Sigma)), which favors the expansion of erythroblast but does not support lymphocytes growth. Cell numbers were counted and medium was refreshed every two days. When the cell number became approximately same or greater over the starting cell number, the MNCs were suitable for reprogramming. All reagents were purchased from Thermo Fisher Scientific if not otherwise specified.

Generation of iNPCs from human adult PB MNCs by episomal vector transfection

The oriP/EBNA1-based episomal vectors EV SFFV-OCT4-2A-SOX2 (SFFV-OS), EV SFFV-MYC-2A-KLF4 (SFFV-MK) and EV SFFV-BCL-XL have been described previously (Su et al., 2013). The process for human iNPC generation is schematically summarized in Figure 1A. Two million PB MNCs were nucleofected with a mixture of the episomal vectors (4 μg SFFV-OS, 4 μg SFFV-MK and 2 μg SFFV-BCL-XL) following the Amaxa 4D-Nucleofector Protocols for Unstimulated Human $CD34^+$ Cells

(Lonza, P3 primary cell 4D-Nucleofector X Kit). After nucleofection, the PB MNCs were recovered in MNC medium for 2 days and plated onto irradiated MEFs on Matrigel-coated 12-well-plate at a density of 2×10^5/well in MEF medium. The medium was replaced the next day with KSR medium (20% KSR in DMEM/F12 supplemented with 1×Glutamax, 1×NEAA, 0.1 mM β-ME, 10 ng/ml bFGF (Pufei) and 0.25 mM NaB (Sigma)). After 5 days, the medium was changed to N2B27 medium (DMEM/F12: Neurobasal (1:1) supplemented with 1×N2, 1×B27, 1× Glutamax and 0.1 mM β-ME) with small molecule chemicals cocktail including 10 μM SB431542 (Selleck), 3 μM CHIR99021 (Selleck), 0.5 mM VPA (Selleck) and 10 μM Forskolin (Selleck). Culture medium was partially changed every two days. Around 20 days after nucleofection, the NPC-like colonies were picked manually and mechanically triturated into small clusters and reseeded on Matrigel-coated 24-well-plates for further expansion and evaluation. For the first two passages, the human iNPCs were cultured in the N2B27 medium supplemented with 10 ng/ml hLIF (R&D system), 3 μM SB431542 and 3 μM CHIR99021. Then the cells were transferred to the NSC medium (N2B27 medium supplemented with 20 ng/ml bFGF and 20 ng/ml EGF (Peprotech)) to achieve a homogeneous morphology. Cells were purified at passage 4 as neurospheres if they failed to show homogeneous morphology. From passage 5, the established human iNPCs were continuously maintained in NSC medium. For all the passages, human iNPCs were detached using Accutase and cultured on Matrigel-coated dishes. For each donor, 6 lines of iNPCs were generated and stably maintained. All reagents were purchased from Thermo Fisher Scientific if not otherwise specified.

RNA-seq and analysis

PB MNCs from donor 1 and 2 and two lines of iNPCs from each donor were randomly chosen for RNA-seq and analysis. Total RNA was extracted using Trizol reagent (Pufei) and RNA-seq libraries were prepared following the method published previously (Chen et al., 2017). Briefly, the RNA was reversed transcribed by SuperScript II reverse transcriptase (Thermo Fisher Scientific). The double-stranded cDNA was amplified using KAPA HiFi HotStart ReadyMix (KAPA Biosystems) and purified using 1: 0.75

ratio of AMPure XP beads (Bechman Coulter). After quantification by Qubit, cDNA was applied to Bioanalyzer 2100 on a High-Sensitive DNA chip (Agilent Bioanalyzer) to check the library size distribution. Amplified cDNA (~5 ng) was then used to construct Illumina sequencing libraries using Illumina's Nextera DNA sample preparation kit following the manufacturer's instructions. All sample libraries were sequenced on HiSeq2500 instrument (Illumina).

Raw reads were mapped to the hg19 version of human genome using TopHat2 version 2.0.4 program (Trapnell et al., 2009). We calculated fragment per kilobase per million (FPKM) as expression level using Cufflinks version 2.0.2 software (Kim et al., 2013). Genes with the FPKM>1.0 in at least one sample across all samples were retained for further analysis and the expression levels were transformed to log-space by using the $\log_2$ (FPKM+1). Differentially expressed genes (DEGs) among different samples were identified using Rankprod (Hong et al., 2006) with P value < 0.05 and fold change > 2. Functional enrichment of gene sets with different expression patterns was performed using the Database for Annotation, Visualization and Integrated Discovery v6.8 (DAVID v6.8) (Huang da et al., 2009). DEG heat maps were clustered by hierarchical clustering and visualized using Java Tree View software (Saldanha, 2004). PCA analysis was performed using R (http://www.r-project.org). Pearson correlation was used to compare the human iNPC lines with published database CORTECON (van de Leemput et al., 2014) and BrainSpan (http://brainspan.org).

In vitro differentiation of human iNPCs

For spontaneous differentiation of human iNPCs into neurons and astrocytes, human iNPCs were dissociated with Accutase and seeded on PDL-Laminin coated 35 mm dish at a density of 2×10^5 cells/dish and differentiated in the neural differentiation medium consisting of B27 medium (Neurobasal medium with 1×B27, 2 mM Glutamax and 0.1 mM β-ME) supplemented with 1 μg/ml Laminin (Sigma), 1 μg/ml FN (Sigma), 10 ng/ml BDNF (Peprotech), 10 ng/ml NT3 (Peprotech), 10 ng/ml IGF-1 (Peprotech), 10 ng/ml CNTF (Peprotech) and 1 μM cAMP (Sigma). At differentiation day 7, the cells were dissociated into single cells by Accutase and reseeded on PDL-Laminin coated 35

mm dish at a density of 2×10^5 cells/dish and further differentiated in the neural differentiation medium with the addition of 0.2 μM Compound E (Millipore) from differentiation day 9 to 19. For oligodendrocyte differentiation, human iNPCs were first treated with SAG (300 nM) (Millipore) for 10 days and then seeded on PDL-Laminin coated 35 mm dish at a density of 1×10^5 cells/dish in the oligodendrocyte differentiation medium (DMEM/F12 with 1×N2, 1×Glutamax, 0.1 mM β-ME, 30 ng/ml T3 (Sigma), 100 ng/ml Biotin (Sigma), 10 ng/ml PDGF-AA (R&D System), 1 μM cAMP, 10 ng/ml IGF-1, 10 ng/ml NT3 and 10 ng/ml CNTF). Half of the medium was changed every two days during differentiation. Differentiated cells were harvested for evaluation at differentiation day 28 (for neuronal or astrocyte differentiation) or day 35 (for oligodendrocyte differentiation). All reagents were purchased from Thermo Fisher Scientific if not otherwise specified.

Immunofluorescence staining

To prepare brain slices for immunofluorescence staining, mice were anesthetized and perfused transcardially with PBS followed by fixative (4% paraformaldehyde in PBS). Brains were removed from the skull, postfixed overnight, and then transferred into a 20% sucrose solution in PBS for 24 hrs for cryoprotection. The brains were then frozen in -80°C for 2 hrs, cryosectioned into 15 μm thick coronal sections and mounted on gelatinized glass slides. Immunofluorescence staining of brain slices and cultured cells was performed as previously described (Gao et al., 2001; Xia et al., 2007). Primary antibodies and dilutions used in this study are shown in Table S1. Alexa Fluro 488, 546, or 633 secondary antibodies (donkey anti-mouse, donkey anti-rabbit, or donkey anti-goat secondary antibodies, Thermo Fisher Scientific) were used as secondary antibodies. DAPI was used to counterstain nuclei. The images were captured with Olympus BX50 or Leica TCS SP8 confocal laser scanning microscope. Images were collected at 1024×1024-pixel in resolution. For quantification of immunofluorescence staining, 5 fields were randomly chosen for each experiment (*in vitro*) or each mouse brain (*in vivo*).

Generation of human iNPCs lines expressing GFP or ChR2-mCherry

The plasmid FUGW containing GFP (a gift from Dr. David Baltimore (Addgene plasmid # 14883)) was used to generate GFP^+ iNPCs (Lois et al., 2002). To generate iNPCs expressing ChR2-mCherry, the ChR2-mCherry fragment was amplified by PCR from the pAAV-EF1a-ChR2-mCherry (a gift from Dr. Minmin Luo, NIBS, China) and subcloned into the lentiviral vector pFuw-TRE to construct the pFuw-TRE-ChR2-mCherry plasmid. The plasmid FUGW or pFuw-TRE-ChR2-mCherry was packaged into lentivirus that was transfected into iNPCs (< passage 10) as previously described (Tiscornia, 2006). After lentiviral transfection, GFP or mCherry positive iNPC cells were sorted using a FACS Arial cell sorter (BD Biosciences) and propagated for at least 5 passages in NSC medium. The GFP^+ or ChR2-$mCherry^+$ iNPCs were then transplanted into mice brain and analyzed at the indicated time.

Mice

In order to avoid the immune suppression treatment on the host mice and make grafted human neural progenitors survive better, the immunodeficient mice, including wild-type (WT) and AD mice, were recruited in this study. The immunodeficient $Foxn1^{-/-}$ mice were purchased from Shanghai SLAC Laboratory Animal Company (Shanghai, China), which served as the WT control. The strain of heterozygous transgenic AD-model mice 5XFAD (Jackson No. 006554) was purchased from Jackson Lab. The immunodeficient $Rag2^{-/-}$ mice were a gift from Dr. Lijian Hui (SIBCB, China). 5XFAD mice were crossed with $Rag2^{-/-}$ mice to obtain $Rag2^{+/-}$/5XFAD mice, which were then self-crossed to generate the $Rag2^{-/-}$/5XFAD immunodeficient AD model mice. Male mice were used in the study. The cell transplantation was performed in immunodeficient WT mice at 2 months of age and $Rag2^{-/-}$/5XFAD mice at 4 months of age. The behavioral tests were performed in $Rag2^{-/-}$/5XFAD with or without grafted human iNPCs at 9-10 months of age. All of the above mice were housed in a pathogen-free facility and all of the animal experiments were carried out following protocols approved by the Animal Ethics Committee of the Shanghai Institutes for Biological Sciences.

Cell transplantation

For transplantation, human iNPCs at passage 15 were dissociated into single cells using Accutase and suspended in neural differentiation medium supplemented with 10% Matrigel at a density of 5×10^4/μl. Bilateral injections of 2 μl single-cell suspension containing 1×10^5 GFP^+ or ChR2-$mCherry^+$ human iNPCs were then targeted to the hippocampus dentate gyrus (DG) region following coordinates relative to Bregma: AP: -1.06 mm; ML: ±1.0 mm; DV: -2.5 mm. The cells were injected into immunodeficient mice $Foxn1^{-/-}$ (2 months old) or $Rag2^{-/-}$/5XFAD (4 months old) using a 5μl Hamilton micro-syringe (33-gauge) at a rate of 0.4 μl/min. Bilateral injections of 2μl neural differentiation medium containing growth factors into hippocampus of $Rag2^{-/-}$/5XFAD mice as the sham/vehicle controls for behavioral task. Mice were anesthetized with Avertin (0.6 ml/25 g body weight), and the surgery was performed on the stereotaxic apparatus (RWD life science).

Acute brain slice preparation

The use and care of laboratory animals complied with the guidelines of the Animal Advisory Committee at the State Key Laboratory of Cognitive Neuroscience and Learning, Beijing Normal University. Immunodeficient WT or AD mice with grafted human iNPCs 2, 4 and 6 months post transplantation were anesthetized with sodium pentobarbital (50 mg/kg) and sacrificed by decapitation. The brain tissues were immediately dissected out and immersed in ice-cold slicing solution (see below). For mice of 6 months post transplantation, we perfused the mice transcardially with ice-cold sucrose-based slicing solution before decapitation to improve the quality of slices. In ice-cold sucrose-based slicing solution (normal aerated artificial cerebrospinal fluid, i.e. ACSF, listed below but with NaCl replaced with equimolar sucrose) that had been bubbled with 95% O_2 and 5% CO_2, tissue blocks containing hippocampus were sliced coronally with a vibratome (Leica VT1000S). Slices (300 μm thick) were collected and incubated at 35 °C in ACSF containing (in mM): NaCl 126, KCl 2.5, $MgSO_4$ 2, $CaCl_2$ 2, $NaHCO_3$ 26, NaH_2PO_4 1.25, and dextrose 25 (315 mOsm, pH 7.4). After 60-min incubation, slices were then incubated at room temperature until use.

Electrophysiological recording

Whole-cell patch-clamp recording was performed in human iNPC-derived neurons on differentiating day 50 (*in vitro*) and in $EGFP^+$ or $mCherry^+$ human iNPC-derived neurons in the coronal brain slices of immunodeficient mice (*in vivo*). The whole-cell recordings were performed with a Multiclamp 700B (Molecular Devices). The cultured cells were patched as previously described (Yue et al., 2015). For the grafted cells, acute slices were transferred to the recording chamber and perfused with aerated ACSF at a rate of 1.2 ml/min. Slices were visualized under upright infrared differential interference contrast microscope (BX51WI, Olympus). We performed recordings from grafted cells, which were identified by their expression of GFP, with patch pipettes filled with Alexa Fluor-594-containing internal solution (in mM): K-gluconate 145, $MgCl_2$ 2, Na_2ATP 2, HEPES 10, and EGTA 0.2 (286 mOsm, pH 7.2). The impedance of patch pipettes for somatic recording was 3-5 MΩ. Some cells showed spontaneous firing after membrane rupture because of their depolarized membrane potential. For these cells, we hyperpolarized them to -70 mV to examine membrane properties, but they were not included in data analysis of resting membrane potential. Recordings with series resistance >30 MΩ were discarded. In current clamp mode, step currents (with steps of 10 pA, 500 ms in duration) were applied to evoke action potentials (APs). Hyperpolarizing current pulses (-10 pA, 500 ms) were injected to test the input resistance. In voltage clamp mode, spontaneous excitatory postsynaptic currents (sEPSCs) were recorded when membrane potentials were clamped at -70 mV (i.e. the reversal potential of IPSCs), while spontaneous inhibitory postsynaptic currents (sIPSCs) were recorded at EPSC reversal potential, 0 mV. The kinetics of PSCs were analyzed with MiniAnalysis 6.03 (SynaptoSoft Inc., NJ, USA).

Optogenetic experiment

For the immunodeficient mice transplanted with ChR2-expressing grafted cells, we used single-photon setup to examine whether there were synaptic connections forming between host and grafted cells. We used a homemade AOD-based rapid laser

stimulation system equipped with a 473-nm blue laser (50 mW; Cobolt Inc., Sweden). The laser beam was coupled to the light path of an Olympus upright microscope and delivered to the slices through a water-immersion 40X objective (0.8 N.A.). Firstly, we patched a grafted cell with ChR2-mCherry expression on the cell membrane and tested whether light stimulation at the perisomatic region could reliably induce APs. Then we recorded a neighboring host cell identified by their firing pattern and morphology (filled with Alexa Fluor-594 through patch pipettes). Whole field random light stimulation was delivered to activate grafted cells. We clamped the recorded cell at -70 mV and 0 mV to examine the excitatory or inhibitory synaptic inputs induced by light stimulation, respectively.

Spontaneous alternation Y-maze task

Spontaneous alternation performance was tested as described previously (Ohno et al., 2006). Each mouse was placed in the center of the symmetrical Y-maze and was allowed to explore freely through the maze during an 8-min session. The sequence and total number of arms entered was recorded. Experiments were done blind with respect to the genotype and experimental conditions of the mice. Percentage alternation is as follows: number of triads containing entries into all three arms/maximum possible alternations (the total number of arms entered minus 2) × 100.

Barnes maze

Barnes maze behavior test was performed as previously described (Sunyer et al., 2007). The maze was 90 cm in diameter with 20 holes equally spaced along the perimeter. One of the holes was designated as the target hole, which led into a darkened escape box. An electric metronome (AROMA, Shenzhen, China) was used as a buzzer to make a noise of 85 dB, which acted as an aversive stimulus that motivate the mice to find the target hole. Visual cues were placed surrounding the maze, which served as the reference points for the mice to locate the target hole. For training trial, all mice received 4 trials per day with an inter-trial interval of 15 min during the first 4 days.

Each trial consisted of 10 s in the disorientation box in the center of the maze, followed by 3-min exploration time to locate the target hole. Mice that failed to escape were gently guided to the target hole. After escaping, they were left in the escape box for 1 min. The probe trail was performed on day 5, when the escape box was covered and mice were allowed to explore the maze for 90 s. The latency to the first encounter of the target hole (primary latency) and the latency to enter the escape box (total latency) were recorded during training trial. The primary latency, duration in target quadrant and the numbers of nose pokes above each hole were recorded in the probe trial.

Field potential recording

Hippocampal recordings procedures were the same as previously described (Cao et al., 2007; Tang et al., 1999; Wang et al., 2008). Briefly, Whole-brain coronal slices (370 μm thickness) containing the hippocampus were cut using a vibroslicer (Vibratome 3000, Vibratome, St Louis, MO, USA) with cold (4 °C) and oxygenated (95 % O_2, 5 % CO_2) modified artificial cerebrospinal fluid (ACSF) containing (in mM): choline chloride 110, KCl 2.5, $CaCl_2$ 0.5, $MgSO_4$ 7, $NaHCO_3$ 25, NaH_2PO_4 1.25 and D-glucose 25 (pH 7.4). The slices were recovered in an incubation chamber with normal ACSF containing (in mM): NaCl 119, $CaCl_2$ 2.5, KCl 2.5, $MgSO_4$ 1.3, $NaHCO_3$ 26.2, Na_2HPO_4 1.0 and D-glucose 11 (pH 7.4, 95 % O_2 and 5 % CO_2) for 60 min at 31 °C. A unipolar tungsten stimulating electrode (FHC, USA) was placed in CA3 region to deliver electro-stimuli. A glass microelectrode (3 MΩ, 0.5 M CH_3COONa) was positioned in the CA1 region to record extracellular field potentials. Test responses were elicited at 0.033 Hz. After obtaining a stable baseline response for at least 15 min, LTP was induced by three trains of theta burst stimulation (TBS) (10 bursts of four pulses at 100 Hz separated by 200 ms).

Measurement of BDNF

The BDNF level was measured in the whole brain and the hippocampus of $Rag2^{-/-}$ /5XFAD with and without grafted human iNPCs following the manufacturer's protocol (Promega). After sacrifice of mice with Nembutal overdose, half brains (without the

cerebellum and olfactory bulb) were taken and hippocampal tissues were dissected from the other half brain. The tissues were quickly frozen on dry ice, then weighed and homogenized on ice in 150 mg/ml T-PER (Pierce) with protease and phosphatase inhibitor cocktails (Sigma). The homogenate was spun at 16,000 g for 1 hour at 4 °C, and the fresh supernatant was used for ELISA analysis.

Statistical analysis

All statistical analyses were performed in GraphPad Prism software (GraphPad 7.0). Cell counting and electrophysiological data were presented as mean ± SD, while BDNF ELISA, behavior test and LTP data were presented as mean ± SEM. Student's t test (two-tailed) was performed for statistical analysis between two groups. One-way or two-way ANOVA with Tukey's multiple comparison post hoc test was used when three or more groups were compared. Sample size (n) values were provided in the relevant text, figures and figure legends. The statistical analyses were obtained from three independent experiments. Statistical significance was set at $*P < 0.05$.

Data availability

All RNA-seq data are available at the Gene Expression Omnibus (GEO) under accession number GSE107806.

REFERENCES:

Cao, X., Cui, Z., Feng, R., Tang, Y.P., Qin, Z., Mei, B., and Tsien, J.Z. (2007). Maintenance of superior learning and memory function in NR2B transgenic mice during ageing. The European journal of neuroscience *25*, 1815-1822.

Chen, J., Suo, S., Tam, P.P., Han, J.J., Peng, G., and Jing, N. (2017). Spatial transcriptomic analysis of cryosectioned tissue samples with Geo-seq. Nature protocols *12*, 566-580.

Dowey, S.N., Huang, X., Chou, B.K., Ye, Z., and Cheng, L. (2012). Generation of integration-free human induced pluripotent stem cells from postnatal blood mononuclear cells by plasmid vector expression. Nature protocols *7*, 2013-2021.

Gao, X., Bian, W., Yang, J., Tang, K., Kitani, H., Atsumi, T., and Jing, N. (2001). A role of N-cadherin in neuronal differentiation of embryonic carcinoma P19 cells. Biochem Biophys Res Commun *284*, 1098-1103.

Hong, F., Breitling, R., McEntee, C.W., Wittner, B.S., Nemhauser, J.L., and Chory, J. (2006). RankProd: a bioconductor package for detecting differentially expressed genes in meta-analysis.

Bioinformatics *22*, 2825-2827.
Huang da, W., Sherman, B.T., and Lempicki, R.A. (2009). Systematic and integrative analysis of large gene lists using DAVID bioinformatics resources. Nature protocols *4*, 44-57.
Kim, D., Pertea, G., Trapnell, C., Pimentel, H., Kelley, R., and Salzberg, S.L. (2013). TopHat2: accurate alignment of transcriptomes in the presence of insertions, deletions and gene fusions. Genome biology *14*, R36.
Lois, C., Hong, E.J., Pease, S., Brown, E.J., and Baltimore, D. (2002). Germline transmission and tissue-specific expression of transgenes delivered by lentiviral vectors. Science *295*, 868-872.
Ohno, M., Chang, L., Tseng, W., Oakley, H., Citron, M., Klein, W.L., Vassar, R., and Disterhoft, J.F. (2006). Temporal memory deficits in Alzheimer's mouse models: rescue by genetic deletion of BACE1. The European journal of neuroscience *23*, 251-260.
Saldanha, A.J. (2004). Java Treeview-extensible visualization of microarray data. Bioinformatics *20*, 3246-3248.
Su, R.J., Baylink, D.J., Neises, A., Kiroyan, J.B., Meng, X., Payne, K.J., Tschudy-Seney, B., Duan, Y., Appleby, N., Kearns-Jonker, M.*, et al.* (2013). Efficient generation of integration-free ips cells from human adult peripheral blood using BCL-XL together with Yamanaka factors. PloS one *8*, e64496.
Sunyer, B., Patil, S., Höger, H., and Lubec, G. (2007). Barnes maze, a useful task to assess spatial reference memory in the mice.
Tang, Y.P., Shimizu, E., Dube, G.R., Rampon, C., Kerchner, G.A., Zhuo, M., Liu, G., and Tsien, J.Z. (1999). Genetic enhancement of learning and memory in mice. Nature *401*, 63-69.
Tiscornia, G., Singer, O. and Verma, I. M. (2006). Production and purification of lentiviral vectors. Nat Protoc *1*, 241-245.
Trapnell, C., Pachter, L., and Salzberg, S.L. (2009). TopHat: discovering splice junctions with RNA-Seq. Bioinformatics *25*, 1105-1111.
van de Leemput, J., Boles, N.C., Kiehl, T.R., Corneo, B., Lederman, P., Menon, V., Lee, C., Martinez, R.A., Levi, B.P., Thompson, C.L.*, et al.* (2014). CORTECON: a temporal transcriptome analysis of in vitro human cerebral cortex development from human embryonic stem cells. Neuron *83*, 51-68.
Wang, H., Feng, R., Phillip Wang, L., Li, F., Cao, X., and Tsien, J.Z. (2008). CaMKII activation state underlies synaptic labile phase of LTP and short-term memory formation. Current biology : CB *18*, 1546-1554.
Xia, C., Wang, C., Zhang, K., Qian, C., and Jing, N. (2007). Induction of a high population of neural stem cells with anterior neuroectoderm characters from epiblast-like P19 embryonic carcinoma cells. Differentiation *75*, 912-927.
Yue, W., Li, Y., Zhang, T., Jiang, M., Qian, Y., Zhang, M., Sheng, N., Feng, S., Tang, K., Yu, X.*, et al.* (2015). ESC-Derived Basal Forebrain Cholinergic Neurons Ameliorate the Cognitive Symptoms Associated with Alzheimer's Disease in Mouse Models. Stem cell reports *5*, 776-790.